FINAL TECHNICAL REPORT

To

NASA Lewis Research Center

Grant NAG3-827

NiAl Alloys for Structural Uses

D. A. Koss

Department of Materials Science and Engineering
The Pennsylvania State University
University Park, PA 16802

SUMMARY

Alloys based on the intermetallic compound NiAl are of technological interest as high temperature structural alloys. These alloys possess a relatively low density, high melting temperature, good thermal conductivity, and (usually) good oxidation resistance. However, NiAl and NiAl-base alloys suffer from poor fracture resistance at low temperatures as well as inadequate creep strength at elevated temperatures. This research program explored macroalloying additions to NiAl-base alloys in order to identify possible alloying and processing routes which promote both low temperature fracture toughness and high temperature strength.

Initial results from the study [D. R. Pank, M. V. Nathal, and D. A. Koss, in MRS Symposium Vol. 133, 1989, pp. 561-66 and D. R. Pank, M. V. Nathal, and D. A. Koss, J. Mater. Res. 5, 1990, pp. 942-949] examined the additions of Fe, Co, and Hf on the microstructure, deformation, and fracture resistance of NiAl-based alloys. Of significance were the observations that (a) the presence of the gamma-prime phase, based on Ni_3Al, could enhance the fracture resistance if the gamma-prime were present as a continuous grain boundary film or "necklace", (b) the Ni-35Al-20Fe alloy was ductile in ribbon form despite a microstructure consisting solely of the B2 beta phase based on NiAl.

The ductility inherent in the Ni-35Al-20Fe alloy was explored further in subsequent studies [J. Kostrubanic, D. A. Koss, I. E. Locci, and M. V. Nathal, MRS Symp. Proc. 213, 1991, pp. 679-684 and J. M. Kostrubanic, J. B. Breedis, D. A. Koss, I. E. Locci and J. M. Poole, to be published in International Symposium on Structural Intermetallics]. Those results confirm the presence of ductility in the Ni-35Al-20Fe alloy after rapid cooling from 750°-1000°C. However exposure at 550°C caused embrittlement; this was associated with an age-hardening reaction caused by the formation of Fe-rich precipitates.

In contrast, to the Ni-35Al-20Fe alloy, exploratory research indicated that compositions in the range of Ni-35Al-12Fe retain the ordered B2 structure of NiAl, are ductile, and do not age-harden or embrittle after thermal exposure. Thus, our recent efforts have focused on the behavior of the Ni-35Al-12Fe alloy.

A second parallel effort initiated in this program was to use an alternate processing technique, mechanical alloying, to improve the properties of NiAl-alloys. Mechanical alloying in the conventional sense requires ductile powder particles which, through a cold welding and fracture process, can be dispersion strengthened by submicron-sized oxide particles. Using both the Ni-35Al-20Fe and Ni-35Al-13Fe compositions, we have been successful in mechanically alloying NiAl-Fe alloys to contain approx. 1 v/o Y_2O_3. Preliminary results indicate that mechanically alloyed and extruded NiAl-Fe + Y_2O_3 alloys when heat treated to a grain-coarsened condition, exhibit (a) improved creep resistance at 1000°C when compared to NiAl, (b) oxidation resistance comparable to NiAl, and (c) fracture toughness values a factor of three better than NiAl. As a result of the research initiated on this NASA program, a subsequent project with support from Inco Alloys International is underway.

As a result of this NASA research program, two M.S. theses and four publications have been written. These are as follows:

(a) M.S. theses (Penn State University)

- Deborah Pank, "The Effect of Alloying on the Microstructure and Mechanical Properties of Rapidly Solidified Nickel Aluminide Alloys"
- James Kostrubanic, "The Influence of Processing and Thermal History on the Properties of NiAl-based Alloys Containing Iron"

(b) Publications (see attachment)

- D. R. Pank, M. V. Nathal, and D. A. Koss, "Deformation Behavior of NiAl-Based Alloys Containing Iron, Cobalt, and Hafnium in High Temperature Ordered Intermetallic Alloys III, MRS Proc. Vol. 133, 1989, p. 561-66.
- D. R. Pank, M. V. Nathal, and D. A. Koss, "Microstructure and Mechanical Properties of Multiphase NiAl-Based Alloys", J. Mater. Res. 5, 1990, pp. 942-949.
- J. Kostrubanic, D. A. Koss, I. E. Locci, and M. Nathal, "On Improving the Fracture Toughness of a NiAl-based Alloy by Mechanical Alloying in High-Temperature Ordered Intermetallic Alloys IV" in MRS Symp. Proc. Vol, 213, 1991, pp. 679-684.

- J. M. Kostrubanic, J. B. Breedis, D. A. Koss, I. Locci, and J. M. Poole "The Influence of Processing and Thermal History on the Properties of NiAl-based Alloys Containing Iron" to be published in Int. Symp. on Structural Intermetallics, Seven Springs, PA 1993.

DEFORMATION BEHAVIOR OF NiAl-BASED ALLOYS CONTAINING IRON, COBALT, AND HAFNIUM.

D.R. PANK+, M.V. NATHAL*, AND D.A. KOSS+
+Dept. Mat. Sci. & Eng., Penn State, University Park, PA 16802
*NASA Lewis Research Center, Cleveland, OH 44135

ABSTRACT

The effects of alloying additions on the mechanical properties of the B2 intermetallic NiAl have been investigated in both the melt-spun ribbon and consolidated, bulk form. The study is based on a matrix of NiAl-based alloys with up to 20 a/o Co and Fe additions and with reduced Al levels in the range of 30 - 40 a/o. Characterization of the melt-spun ribbon by optical and scanning electron microscopy indicates a range of microstructures: single phase β, γ necklace phase surrounding either martensitic or β grains, and a mixture of equiaxed martensitic and γ grains. Bend ductility is present in melt-spun and annealed ribbons exhibiting the γ necklace structure and in a single phase β material containing 20 a/o Fe.

The analysis of compressive flow behavior on consolidated, bulk specimens indicates that the single phase β alloys exhibit a continuous decrease in yield stress with increasing temperature and profuse microcracking at grain boundaries. In contrast, multiphase (γ + either martensite or β) alloys tend to display a peak in flow stress between 600 and 800K with little or no signs of microcracking. In general, heat treatments which convert the martensitic grains to β + γ result in improved strength at temperatures above 600K and better resistance to crack initiation. These results are discussed in terms of the effects of β, martensite and γ on the yield stress and flow behavior of NiAl-based alloys.

INTRODUCTION

Ordered intermetallic compounds are of interest for high temperature applications because of their potential for high temperature stability, high creep resistance, high melting point, and (in many cases) low density. Among the intermetallics, compounds based on the aluminides are of particular interest because many possess oxidation resistance due to their ability to form protective oxide films on surfaces. Of the aluminides, alloys based on NiAl offer considerable potential because they exhibit an attractive combination of the properties listed above. However, a major problem with most intermetallic aluminides, and NiAl-based alloys in particular, is their low ductility and tendency to fracture in a brittle manner at low temperatures. Therefore, the general goal of this work is to utilize processing and compositional control to obtain NiAl-based alloys which exhibit both low temperature fracture resistance as well as good strength at high temperatures.

Utilizing rapid solidification techniques, previous investigators have added Fe and Co to NiAl-based alloys and have observed increases in ductility in rapidly solidified wire specimens [1]. The ductility increases have been attributed to grain size refinements, elimination of grain boundary segregation, and also increases in alloy homogeneity [1]. However, it is known that Cr and Mn additions to NiAl alloys activate <111> slip [2]. Thus, it is possible that the Fe additions cause a similar effect; this is currently being investigated by Guha and Baker [3]. If so, the Von Mises criterion for active deformation systems near grain boundaries would be satisfied, possibly resulting in polycrystalline tensile ductility. Co is known to stabilize the β phase in solid solutions based on the intermetallic NiAl, and it depresses the martensitic transformation to lower temperatures [4]. In addition, hafnium is a common alloying addition in advanced Ni-based superalloys and Ni_3Al alloys and may serve to refine a multiphase (γ + either martensite or β) microstructure, which should enhance the likelihood of ductility. This investigation extends work [1] previously performed on rapidly solidified material and compliments separate, on-going programs [3,5] in order to study NiAl-base alloys with Co, Fe, and Hf additions. These alloys have been examined both in the melt-spun condition and as bulk materials consolidated by hot pressing. Both microstructural characteristics and compressive flow behavior are reported.

Mat. Res. Soc. Symp. Proc. Vol. 133. © 1989 Materials Research Society

EXPERIMENTAL PROCEDURES

Several materials and processing techniques have been utilized in this investigation. The alloys range in composition such that single phase β as well as multiphase β + γ alloys with varying phase morphologies have been obtained. These are denoted as single phase β, necklace γ, and blocky/irregular γ'. The chemical compositions are listed in Table 1; all compositions are in atomic percent unless otherwise noted.

Table 1
Alloy Compositions

Single Phase β	Necklace γ	Blocky/Irregular γ'
Ni 40Al 18Co	Ni 35Al 18Co	Ni 30Al 9Co 1Hf
Ni 35Al 20Fe	Ni 31Al 18Co	Ni 30Al 9Co
Ni 34Al 9Co 11Fe	Ni 36Al 9Co	

Free jet melt spinning has been performed at NASA-Lewis to produce the rapidly solidified ribbon material. Room temperature bend testing of both as-spun and heat-treated ribbons has been accomplished by bending the ribbon around a mandrel of successively smaller diameter until failure occurs. The strain at failure ε_f may be readily determined from the minimum bend radius and ribbon thickness [6]. For each condition, half of the eight to ten tests have been conducted with the wheel side of the ribbon as the outer bend surface and the other half with the free side of the ribbon as the outer bend surface.

Before consolidation of the melt-spun ribbons into bulk specimens, the material was pulverized in a Waring blender for approximately 10-15 minutes. Particle size ranged from 50 μm to 2 cm. The pulverized ribbon was then consolidated by hot pressing at 1523K for 7 hours at a pressure of 3.3 ksi with a subsequent slow cooling of four hours to room temperature. Compression samples were prepared by electron discharge machining into rectangular specimens having the dimensions of 3.8 x 3.8 x 10.2 mm. Subsequently, the specimens were mechanically polished to a surface finish of 0.05 μm. Compression testing on the consolidated material was performed in air at 300, 600, 800, and 1000K at an engineering strain rate of 2×10^{-3} s^{-1}. Optical and scanning electron microscopy were performed on specimens etched in a solution of 33% nitric acid, 33% acetic acid, 33% water, and 1% hydrofluoric acid.

RESULTS AND DISCUSSION

(a) Rapidly Solidified Melt Spun Ribbon Material

A very significant observation is the presence of bend ductility at room temperature in ribbons of the single-phase β alloy Ni 35Al 20Fe in the as-spun condition and after several different annealing treatments. The presence of ductility may be due to the Fe-induced operation of different slip systems with a <111> slip direction [2,3] as well as the lack of grain boundary compatibility constraints when the grain size is comparable to ribbon thickness, as was the case for the annealed specimens. In addition, the Ni 31Al 18Co alloy in which a film of the γ' phase surrounds martensitic grains also exhibits significant bend ductility. All of the other alloys are brittle in ribbon form.

The microstructure of the Ni 31Al 18Co alloy can be varied significantly by heat treatment, and this in turn affects ductility. Specifically, the following observations have been made on the ribbon specimens: (a) a fully martensitic structure which is obtained by quenching from 1373K exhibits no room temperature bend ductility and intergranular fracture; (b) a thin film of γ, ~1μm thick along grain boundaries in a martensitic matrix, forms after a 30 minute cool from 1373K and imparts an average plastic bend ductility of 3.2%; and (c) an even thicker but irregular γ' film, ~4μm, accompanied by a dispersion of γ within the martensitic grains is obtained after a four hour cool from 1373K. This microstructure has the largest volume fraction of γ (17%) and exhibits the greatest average plastic bend ductility (6.6%) at room temperature. The microstructures with γ at the boundaries and/or within the grains fail by what appears to be fracture along the martensite/γ interfaces.

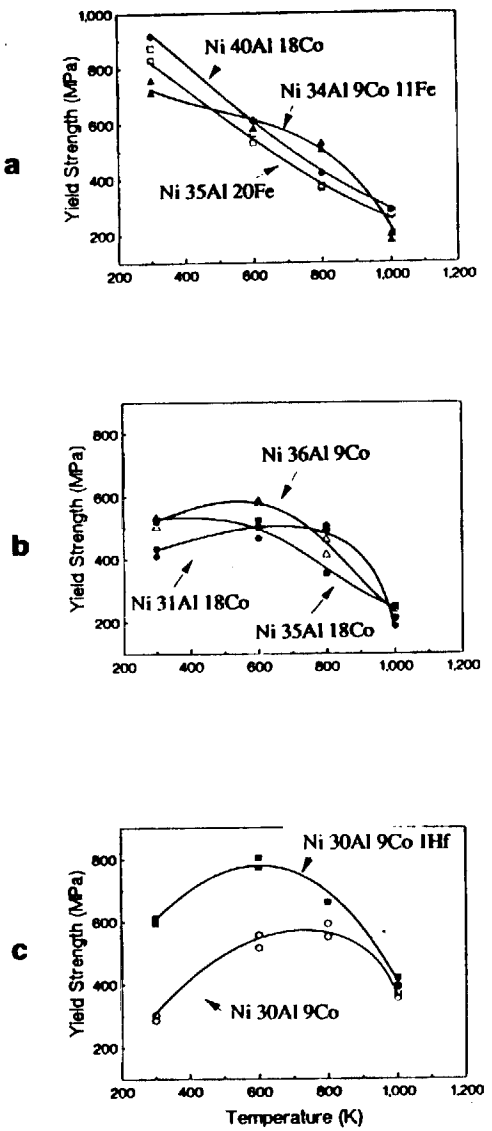

Figure 1. The dependence of σ_y on temperature for (a) single phase beta, (b) necklace γ', and (c) blocky/irregular γ' alloys.

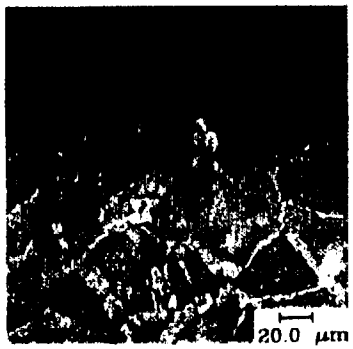

Figure 2. Optical micrographs of the necklace γ alloy Ni 31Al 18Co in the as-hot-pressed condition.

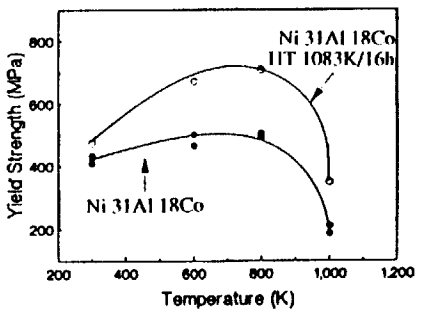

Figure 3. The dependence of σ_y on temperature for the annealed Ni 31Al 18Co alloy.

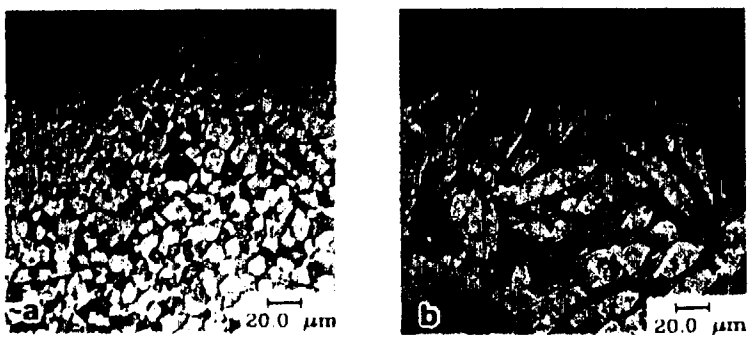

Figure 4. Optical micrographs of the blocky/irregular γ alloys in the as-hot-pressed condition (a) Ni 30Al 9Co 1Hf and (b) Ni 30Al 9Co.

(b) Consolidated, Bulk Material

Figure 1 shows the dependence of the yield stresses with temperature for the three different microstructural conditions investigated in this study. In all cases, the materials are in the fully dense, as-hot-pressed condition. As is the case for near equiatomic NiAl [7], the yield strength vs. temperature curves for the single phase β alloys, Fig. 1a, show that while the materials exhibit high yield strengths at low temperatures, the yield strength decreases rapidly with increasing temperatures. The Ni 35Al 20Fe alloy, which shows prominent bend ductility in ribbon form, exhibits extensive intergranular microcracking after testing to ~5% compressive strain. It should be noted that after consolidation, the grain sizes of the single phase β alloys are quite large, ranging from 50 to 65 μm.

Three of the NiAl + Co alloys corresponding to Fig. 1b form necklace γ + (β or martensite) microstructures after hot pressing. As shown in Fig. 2 for Ni 31Al 18Co, these microstructures consist of a continuous γ film surrounding martensitic grains for the Ni 31Al 18Co and Ni 36Al 9Co alloys and a discontinuous γ film surrounding β grains for the Ni 35Al 18Co alloy. It should be noted that these three alloys contain 19, 11, and 2 volume percent of the γ phase, respectively. The grain size after consolidation for the three necklace structures range from 50 to 62 μm. These microstructures show a positive temperature dependence of the yield strength with temperature up to 600-800K, after which the yield stress decreases. As shown in Fig. 1b, this behavior is very likely due to the influence of the γ, which characteristically exhibits a peak in yield stress at 850-1100K [8]. Microcracking did occur in these necklace γ alloys after compression testing to 5% strain.

A study of the effects of heat treatment has also been performed on the Ni 31Al 18Co alloy in its consolidated form. As shown in Fig. 3, a heat treatment of 16 hours at 1073K results in a 30% increase in strength at temperatures above 600K. This increase in strength is due to a change from the as hot-pressed martensite + γ structure with 19 volume percent γ to a β + γ structure with ~60 volume percent γ. It should be noted that no cracking occurs in the β + γ structure after testing to ~7% compressive strain.

The effects of the γ phase on the yield strength behavior in the materials with the blocky/irregular γ structures, shown in Fig. 1c, is much more apparent due to the increased γ volume fractions in these two alloys. In the Ni 30Al 9Co 1Hf alloy, the presence of the Hf reduces the scale of the microstructure by a factor of seven and also increases the volume fraction of γ from 51% to 63% compared to the Ni 30Al 9Co alloy, as seen in Fig. 4. The effect of the refinement in microstructure as well as the solid solution hardening of the γ are very apparent in the much higher yield strengths at lower temperatures (<600K) of the Hf-containing alloy. It should be noted that after room temperature testing to ~5% compressive strain, there is no cracking in these two alloys.

CONCLUSIONS

In ribbon form, the single phase Ni 35Al 20Fe alloy is ductile despite a microstructure consisting of solely the B2 beta phase. Of the seven other NiAl-based alloys examined, only the Ni 31Al 18Co alloy exhibited measurable ductility prior to fracture. Its microstructure consists of a continuous film of γ along grain boundaries in an otherwise martensitic or β structure.

In bulk, hot-pressed form, the single phase NiAl-based alloys show a rapid decrease in yield strength with increasing temperature and a tendency for profuse microcracking when testing in compression at 5% strain. The multiphase (γ + martensite or β) alloys show an increase in yield strength with increasing temperature due to the presence of the γ. Microcracking does not occur during compression testing in the blocky/irregular γ structures. However, microcracking does occur after testing to 5% strain in the necklace γ structures. An increase in strength by ~30% and the elimination of cracking is achieved in the Ni 31Al 18Co alloy after annealing treatments which convert the martensitic matrix to γ + β.

REFERENCES

1. A. Inoue, H. Tomioku, and T. Masumoto: Met. Trans., 14A, 1983, p. 1367.
2. C.C. Law and M.J. Blackburn, "Rapidly Solidified Lightweight Durable Disk Material" (Report FR-18674-4, Pratt and Whitney Group, 1985).

3. S. Guha and I. Baker: private communications.
4. V.S. Litvinov and A.A. Arkhangel'skaya: Phys. Met. Metall., 44, 1978, p. 131.
5. C.C. Law and M.J. Blackburn, "Lightweight Disk Alloy Development" (Reports FR-19577-1 through 5, Pratt and Whitney Group, 1987-1988).
6. D.J. Gaydosh and M.A. Crimp in High Temperature Ordered Intermetallic Alloys, (eds. C.C. Koch, C.T. Liu, and N.S. Stoloff), Pittsburg, PA: Materials Research Society, 1985, p. 429.
7. R.T. Pascoe and C.W.A. Newey: Metal Sci., 5, 1971, p. 50.
8. D.P. Pope and S.S. Ezz: International Metals Review, 29, 1984, p. 136.

DEFORMATION OF A NI-AL-FE GAMMA/BETA ALLOY

R.D. FIELD*, D.D. KRUEGER*, AND S.C. HUANG**
*GE Aircraft Engines, 1 Neumann Way, Cincinnati, OH, 45215
**GE Corporate Research and Development Laboratories, PO Box 8, Schenectady, NY, 12301

ABSTRACT

Room temperature tensile tests were performed on annealed melt-spun ribbons of a 50Ni-20Al-30Fe alloy. The ribbons were found to possess a duplex structure consisting of fcc γ and B2 β grains and exhibited tensile elongations in excess of 10% while still maintaining good strength. The tested specimens were found to contain high dislocation densities in both the γ and β grains, with no indications of stress-induced martensite formation. Dislocation analysis revealed that the vast majority of dislocations in the β have <100> Burgers vectors; however, <111> dislocations were also observed. Slip transfer was often facilitated by specific orientation relationships between the γ and β grains.

BACKGROUND

For high temperature structural applications, such as those requiring Ni-base superalloys, β-NiAl may offer significant advantages in specific strength, use temperature capability, and oxidation resistance. Similar incentives have already encouraged a great deal of study on Ni_3Al. The major barrier to structural use for either system has been inadequate ductility at ambient to moderate temperatures. Unlike the Ni_3Al system, which possesses a sufficient number of independent slip systems and can be rendered ductile by micro-alloying [1-3], the brittleness of NiAl arises from inherent crystal structure characteristics; that is, von Mises plasticity criterion for polycrystalline flow is not satisfied [4]. At temperatures greater than about 500°C, polycrystalline, near stoichiometric NiAl becomes ductile [5]. Plasticity at ambient temperature has been reported for single crystal NiAl, when tested in compression [5-7], and polycrystalline rapidly solidified ribbons when tested in bending and tension [8]. However, strain to fracture for the polycrystalline materials was only about 2%, still inadequate for most structural applications.

Recent work on NiAl has indicated that an attractive approach for improving the ambient ductility of polycrystalline materials is to select Ni-rich Ni-Al-X ternary alloys that form dual phase structures. The advantages of these aluminides should fall between those of NiAl and Ni_3Al, with the opportunity for more immediate structural applicability than NiAl. In the study of Inoue et al. [9], dual phase Ni-Al-Fe alloys processed by melt quenching exhibited as much as 17% strain to fracture at ambient temperature. This ductile behavior was not well understood, and was attributed to the combination of fine grain size, a depression of the development of order, and the suppression of grain boundary segregation.

In the present investigation, the structures, tensile properties, and deformation features in annealed ribbons of Ni-Al-Fe alloys with 20 at % Al and 20-40 at % Fe are being studied. This range in composition considers the β+γ (disordered fcc) and β+γ+γ' phase fields. In this paper, results from a 50Ni-20Al-30Fe alloy are presented.

EXPERIMENTAL PROCEDURE

The material was prepared by a melt spinning technique. A 60g sample was melted in an alumina crucible and melt spun onto an H-12 tool steel wheel, producing a ribbon about 40-70 μm in thickness and approximately 6mm in width. The ribbons were encapsulated in quartz

Mat. Res. Soc. Symp. Proc. Vol. 133. © 1989 Materials Research Society

Microstructure and mechanical properties of multiphase NiAl-based alloys

D. R. Pank[a)]
Department of Materials Science and Engineering, The Pennsylvania State University, University Park, Pennsylvania 16802

M.V. Nathal
NASA Lewis Research Center, Cleveland, Ohio 44135

D. A. Koss
Department of Materials Science and Engineering, The Pennsylvania State University, University Park, Pennsylvania 16802

(Received 15 September 1989; accepted 16 January 1990)

The effect of the γ' phase on the deformation behavior fracture resistance of melt-spun ribbons and consolidated bulk specimens of a series of NiAl-based alloys with Co and Hf additions has been examined. The morphology, location, and volume fraction of the γ' phase are significant factors in enhancing the fracture resistance of the normally brittle NiAl-based alloys. In particular, the results indicate that a continuous grain boundary film of γ' can impart limited room temperature ductility regardless of whether B2 or $L1_0$ NiAl is present. Guidelines for microstructure control in multi-phase NiAl-based alloys are also presented.

I. INTRODUCTION

Aluminide alloys are currently the subject of considerable interest as a basis for a new generation of structural materials. Alloys based on NiAl are especially attractive because of their relatively low density, comparatively high melting temperature, and excellent high temperature oxidation resistance. Unfortunately, aside from a few isolated reports, previous studies indicate that single phase NiAl-based alloys are brittle at room temperature.[1-6] Published information also indicates that under certain conditions the presence of the γ' phase based on $L1_2$ Ni_3Al may impart some ductility to the otherwise brittle B2 NiAl phase or its $L1_0$ martensitic derivative.[7-10] However, previous results show that the presence of γ' does not guarantee ductility in an alloy based on NiAl.[9] The purpose of this communication is to provide additional evidence for the enhanced fracture resistance of NiAl-based alloys containing a γ' "ductilizing" phase and to identify guidelines for the optimum morphology, distribution, and location of that phase. The observations are based on the behavior of rapidly solidified ribbon specimens, bulk hot-pressed material, and hot-extruded specimens. The use of melt spinning as the initial processing step was based on two reasons. First, previous work[8] showed attractive properties of similar alloys in rapidly solidified form, although it was unclear whether these properties were the result of the alloy composition or from the rapid cooling rates. Second, it is important to observe the behavior of rapidly solidified material after subsequent high temperature consolidation and exposure. For materials intended for high temperature structural use, the primary benefits of rapid solidification are expected to be improved homogeneity and the opportunity for a refined grain size or distribution of dispersoids. Although these latter two aspects were not specifically investigated in this study, it is anticipated that a suitable dispersoid could be added to an alloy as a next step in development.

II. EXPERIMENTAL PROCEDURE

Five alloys have been examined in this study. In atomic percent, their compositions are (1) Ni35Al18Co, (2) Ni31Al18Co, (3) Ni35Al9Co, (4) Ni29Al9Co1Hf, and (5) Ni30Al9Co as determined by inductively coupled plasma spectroscopy. Chemical analysis of the specimens shows a slight variation in compositions after different processing but in all cases the actual compositions are within ±1 at.% of the concentrations listed above. Oxygen levels were measured at about 120 ppm (wt.%) in ribbon form and 160 ppm after consolidation, while C levels were below the detectability limit of 100 ppm in both ribbon and consolidated forms. Liquidus and solidus temperatures were measured by differential thermal analysis and were found to be independent of heating rate between 2 and 20 K/min.

Free jet melt spinning was performed at NASA-Lewis to obtain ribbons approximately 2 to 3 mm wide and 20 to 40 μm thick. Room temperature bend testing of both as-spun and heat-treated ribbons was accomplished by bending the ribbon around mandrels of successively smaller diameters until failure occurred. The

[a)]Current address: General Electric Aircraft Engine Business Group, Lynn, Massachusetts 02176.

maximum strain at failure was determined from the minimum bend radius and the thickness of the ribbon bent around the mandrel.[11] For each condition, eight to ten tests were performed, half with the wheel side of the ribbon as the outer bend surface and the other half with the free side of the ribbon as the outer bend surface.

Consolidation of all of the alloys was accomplished by hot pressing. Before consolidation, the ribbon material was pulverized in a Waring blender for 10–15 min in order to produce flakes of 50 μm to 2 mm in length. The flake material was then consolidated by hot pressing at 1523 K for 7 h at 23 MPa in graphite dies to a fully dense condition. Some of the Ni31Al18Co and Ni29Al9Co1Hf alloys were hot pressed and then subjected to additional processing by extrusion at 1373 K using an area reduction ratio of 12 to 1.

The consolidated material was tested in compression and, in the case of the extruded material, tension as well. Compression specimens were prepared by electron discharge machining into rectangular specimens having the dimensions of 3.8 × 3.8 × 10.2 mm. Before testing, the specimens were mechanically polished to a surface finish of 0.05 μm. Compression tests were performed in air at 300, 600, 800, and 1000 K at an initial engineering strain rate of 2×10^{-3} s^{-1}. Round tensile specimens with a gage diameter of 3.2 mm and gage length of 37.8 mm were centerless ground with the specimen axis corresponding to the extrusion direction. Prior to testing, the tensile bars were electropolished in a 10% perchloric/methanol electrolyte at 253 K.

III. RESULTS AND DISCUSSION

A. Microstructural development

The microstructures of the alloys were significantly influenced by both composition and processing history. In general, the microstructures consisted of NiAl grains, which were present as either β (B2) or martensite ($L1_0$), and γ' ($L1_2$) as the major second phase. The alloys examined can be subdivided into two groups which characterize the morphology of the γ' phase. First, alloys with a "necklace γ' structure" include Ni31Al18Co, Ni35Al18Co, and Ni35Al9Co, and tend to contain γ' which is present as a film surrounding either B2 or $L1_0$ grains. Figure 1(a) shows an example of a necklace γ' structure in a martensite matrix. The γ' is formed by a solid state precipitation reaction from the β phase which is stable at high temperatures; this allows substantial manipulation of the microstructure by subsequent heat treatment. For example, heat treating above the γ' solvus and water quenching results in dissolution of the γ' and martensitic structure forming upon quenching, such as is shown in Fig. 1(b). Slow cooling or intermediate temperature annealing results in γ' precipitation which occurs preferentially at grain boundaries but intragranularly as well; see Fig. 1(c). The intragranular γ' has an acicular morphology and frequently precipitates on martensite twin boundaries. The second group of alloys may be described as having "blocky/irregular γ' structures" and includes the two alloys Ni29Al9Co1Hf, and Ni30Al9Co where representative microstructures are shown in Fig. 2. These alloys are characterized by high volume fractions (>50%) of γ' in the form of nearly equiaxed grains interspersed with the NiAl-based constituent. In this case, both γ' and β form from the melt. Because these alloys are in the two phase $\gamma' + \beta$ field at all temperatures below the solidus, the γ' cannot be completely dissolved by any solid state solutionizing treatment. However, additional γ' can precipitate from the solid during cooling or annealing, since the $\beta/\gamma' + \beta$ phase boundary is curved.

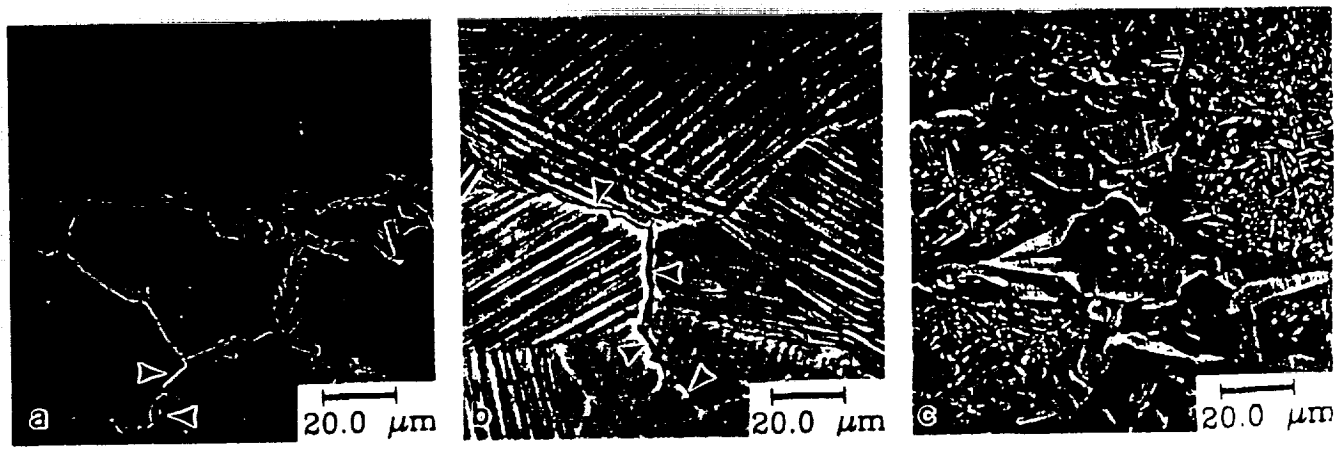

FIG. 1. Microstructures of the hot-pressed necklace γ' alloy Ni31Al18Co: (a) after a 1523 K/0.5-h anneal and quench, (b) in the as-hot-pressed condition, and (c) after a 1073 K/16-h anneal. The specimens have been deformed ~5% in compression at room temperature; note the cracks denoted by the arrows in (a) and (b).

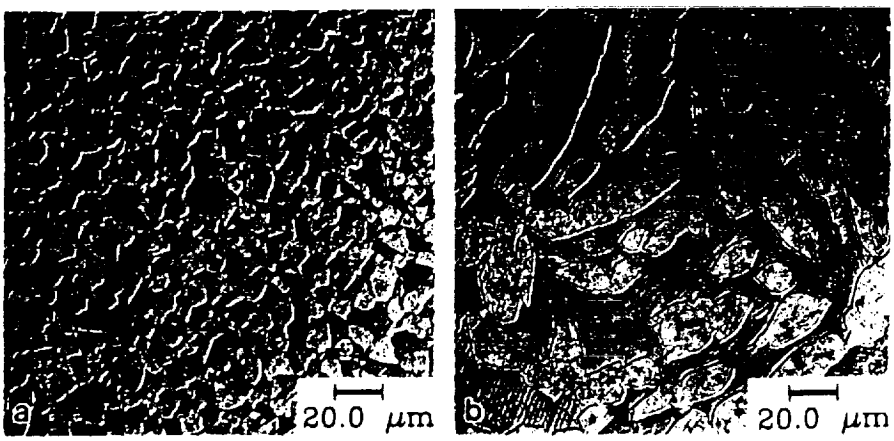

FIG. 2. Microstructures of the blocky/irregular γ' alloys (a) Ni29Al9Co1Hf and (b) Ni30Al9Co after hot pressing.

The Co and Al contents have strong influences on the microstructures of the alloys. Figure 3 displays the volume fraction of γ' as a function of temperature for the various alloys. These data were determined by aging hot-pressed specimens for 24 h at selected temperatures and water quenching. It is quite possible that the precipitation of γ' could not be totally suppressed by the water quench. For example, it is likely that the γ' solvus for the (Ni35Al)–Co alloys is near 1300 K and that the small amounts of γ' measured in samples aged above 1300 K actually precipitated during quenching. Nevertheless, the values shown in Fig. 3 indicate that wide variations in microstructure can be obtained by changes in heat-treatment temperature. Figure 3 shows that at a given temperature and Co level, lower Al levels result in larger amounts of γ , as would be expected. Comparing the phase amounts present in the (Ni35Al)–Co and (Ni30Al)–Co with those expected based on the Ni–Al binary system,[12] it can also be seen that Co is a β-phase stabilizer; its presence favors β over γ' at a constant Al level. This implies that Co substitutes for Al in NiAl to some degree. Energy dispersive spectroscopy (EDS) analysis using the SEM indicated that Co partitioned approximately equally between β and γ'. Co content also affects the martensite transformation in these alloys, as has been reported previously.[13,14] For example, for the (Ni35Al)–Co alloys, increasing Co from 9 to 18% caused the β phase to be retained after quenching instead of martensite; see Fig. 1(d). This effect is consistent with the relationship for the martensite start temperature (M_s) and Co content developed previously,[14] which would predict a change in M_s from 400 to 166 K as Co content changes from 9 to 18%. Finally, none of these Co containing alloys showed any evidence of Ni_5Al_3 formation, even after prolonged aging at low temperature.[15] Several microstructural parameters of these alloys are listed in Table I.

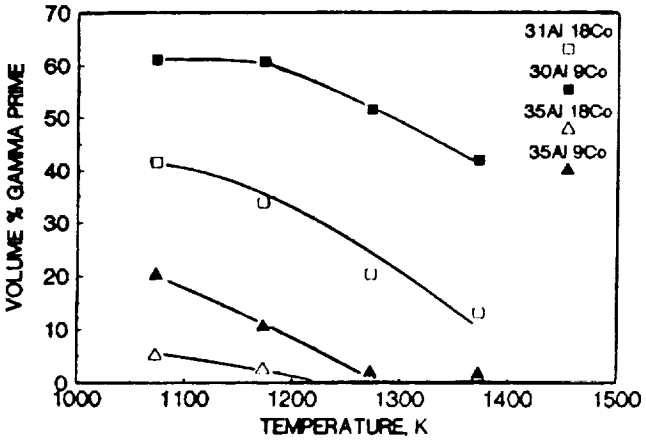

FIG. 3. The volume percent of γ' phase in selected NiAlCo alloys after quenching from the indicated temperatures.

Microstructures of both melt-spun ribbon and consolidated pieces were strongly dependent on heat-treatment temperature and subsequent cooling rate. In the as-spun condition the necklace-type alloys had grain sizes of about 15 μm (as compared to 50–62 μm after hot pressing) and contained some γ' at the grain boundaries, implying that the nucleation and growth of the γ' was relatively rapid. In contrast, the blocky/irregular γ' alloys, especially the Hf-containing alloy Ni29Al9Co1Hf, exhibited finer structures in the as-spun condition, about 5 μm grain sizes as a result of their different solidification mode. The addition of Hf resulted in a significant refinement of the microstructure in both the as-spun condition and after subsequent annealing. EDS analysis showed that Hf partitions strongly to the γ' phase, which would indicate that interface mobility and thus microstructural coarsening would be limited by Hf diffusion.

After consolidation through hot pressing at 1523 K, all of the necklace γ' alloys exhibit grain growth to grain sizes of about 55 μm; see Table I. In general, prior ribbon surfaces, which could be identified by stringers of oxide particles, were not very noticeable and did not appear to restrict grain growth. The morphology of the

TABLE I. Microstructures of NiAl-based alloys.

Alloy	As-spun ribbon microstructure		As-hot-pressed microstructures		γ' Volume fraction				
	Phases	Grain size (μm)	Phases	Grain size (μm)	As-hot-pressed	Annealed 800 °C	M_s[a] K	Solidus	Liquidus
Ni31Al18Co	M + γ'	15	M + γ'	60	19	42	750	1668	1640
Ni35Al18Co	β	10	β + γ'	50	2	5	166	1718	1758
Ni35Al9Co	M	8	M + γ'	60	11	20	400	1718	1738
Ni30Al9Co	M + γ'	5	M + γ'	65	51	61	980	1663	1691
Ni29Al9Co1Hf	M + γ' +Hf-rich pptes	4.0	M + γ'	10	63	...	...	1665	1702

[a]M_s temperatures were calculated using the analysis by Russell and Blackburn.[14]

γ' ranges from about 19 vol.% γ' in a relatively thick (3–15 μm) continuous necklace surrounding martensitic grains in Ni31Al18Co [Fig. 1(a)] to about 2 vol.% γ' in thin ($\leq$ 2 μm) discontinuous film around B2 grains in Ni35Al18Co. The Ni35Al9Co alloy was characterized by $L1_0$ grains and 11 vol.% of γ' in a grain boundary necklace very similar to that in Fig. 1(a). Both blocky/irregular γ' alloys contained γ' in combination with martensite grains, as indicated in Table I and shown in Fig. 2.

The microstructures of the extruded Ni31Al18Co and Ni29Al9Co1Hf alloys are shown in Fig. 4. At the extrusion temperature of 1373 K, both alloys consist of two phase γ' + β microstructures, and the γ' elongates during the deformation. In the as-extruded condition the necklace alloy displayed a discontinuous grain boundary film, but annealing at 1073 K allowed additional γ' to form at the boundaries.

B. Microstructure-property relationships

1. Ribbon material

Of the necklace γ' alloys, the Ni35Al18Co and Ni35Al9Co alloys are brittle in ribbon form in both the as-spun conditions and after annealing at 1073 K and 1273 K for 2 h. In these cases, a relatively small volume fraction (<6 vol.%) of the γ' phase is present as thin ($\leq$1 μm), discontinuous particles located at the grain boundaries. Unlike the other two necklace γ' alloys, ribbons of the Ni31Al18Co alloy exhibit plastic bend ductility of 3.5 to 6.7% in the melt-spun as well as annealed conditions. In these microstructural conditions, roughly 20–25% γ' is present in the annealed conditions, most of it being located as continuous films $\geq$1 μm thick along the grain boundaries, such as in Fig. 1(a).

The microstructure and ductility of the Ni31Al18Co alloy can also be varied by the rate of cooling from

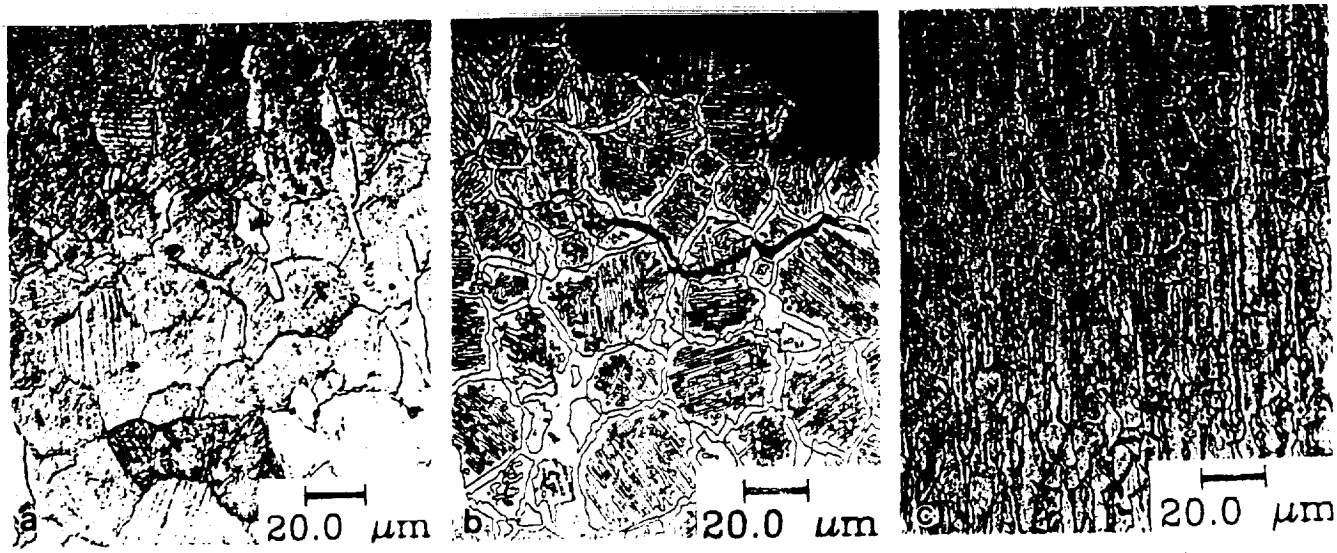

FIG. 4. Optical micrographs of Ni31Al18Co alloy in (a) the as-extruded condition and (b) after a subsequent anneal of 1073 K/96 h. Fig. (c) is of the Ni29Al9Co1Hf alloy in the as-extruded condition. All micrographs are of longitudinal sections and (b) is located adjacent to the fracture surface of a tensile specimen; note cracks.

1373 K. The fully martensitic structure obtained by quenching this alloy is brittle, whereas slow cooling to form a continuous γ' film with a thickness of roughly 1 μm (30-min cool) or 1–6 μm (4-h cool) surrounding the martensitic grains imparts ductility up to a maximum outer fiber strain of 6.6% at room temperature. In the latter case, the microstructure appears similar to the hot-pressed counterpart in Fig. 1(a). Thus, the presence of thick, continuous grain boundary films of the γ' phase is beneficial to room temperature ductility and fracture resistance of the necklace γ' alloys. These results appear to be consistent with those observed elsewhere on multiphase arc-melted and cast NiAl alloys.[9]

In the ribbon form, both of the blocky/irregular γ' alloys, Ni29Al9Co1Hf and Ni30Al9Co, tend to be brittle both in the melt-spun condition and after annealing at 1073 K. This is despite a large amount of γ' phase (50–60 vol.%), the presence of either martensite, and, in the case of the Hf-containing alloy, a very refined (<1 μm) columnar-grained microstructure. The only evidence of ductility in these high-volume-fraction γ' alloys occurred in the Ni30Al9Co alloy annealed at 1273 K; in this case, the microstructure consisted of nearly 60% γ' as a continuous constituent separating martensitic grains and it exhibited roughly 5% bend ductility. Thus, large amounts of γ' phase do not always ensure ductility even in reasonably fine microstructures of less than 1 μm grain size of either β or martensite, although most multiphase alloys with high volume fractions of γ' phase tend to be ductile.

2. Bulk, hot-pressed material

The compressive true stress–true strain behavior and its dependence on temperature are shown in Figs. 5 and 6; several aspects are noteworthy. First, as noted elsewhere,[9] the presence of even a small amount of γ' such as 11% in Ni35Al9Co, can cause the yield stress (defined at 0.2% offset) to increase slightly or to be relatively independent of temperature from room temperature to 600–800 K; note Fig. 5(b). The effect of γ' on the flow behavior is more pronounced at higher volume fractions (>50%), as is shown in Fig. 6 for the case of the alloys with the blocky/irregular gamma-prime microstructures. In this case, the yield stresses increase significantly with increasing temperature to the 600–800 K range, as is shown in Fig. 7. In addition, the presence of Hf reduces the scale of the microstructure by a factor of about seven, for reasons discussed earlier. As a result of a refined microstructure and a very strong Hf-induced solid solution hardening of gamma-prime,[16,17] a comparison of Figs. 6(a) and 6(b) shows that the Hf-containing alloy displays ≈300 MPa higher yield stresses in the 300–600 K regime; at higher temperatures the effect diminishes as the specimens begin to exhibit creep-type deformation behavior.

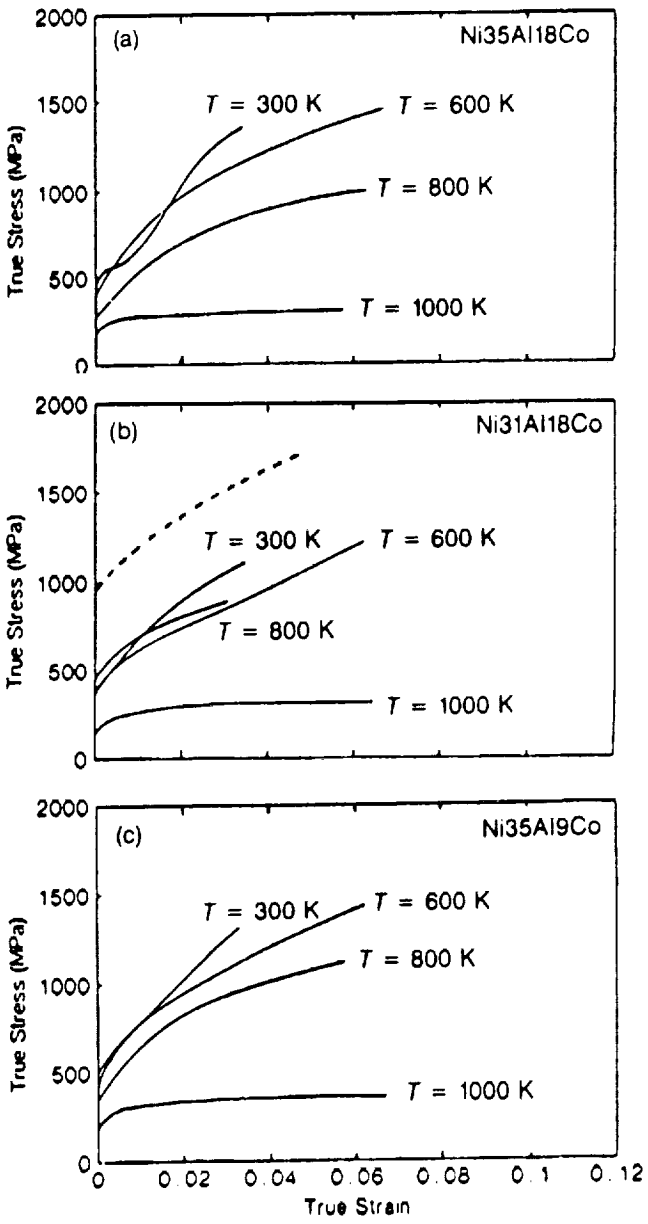

FIG. 5. True stress–true strain behavior for the necklace γ' alloys: (a) Ni35Al18Co, (b) Ni31Al18Co, and (c) Ni35Al9Co. Tests are performed in compression and except for the dotted line in (b) are of as hot-pressed specimens. The dotted line data are for a hot-extruded specimen.

The second noteworthy aspect of the flow response in Fig. 5 is related to the fact that, despite a low calculated M_s-value of 166 K for the Ni35Al18Co alloy,[14] x-ray diffraction confirms that the B2 phase transforms to martensite during deformation at room temperature. This results in the characteristic stress-strain response at 300 K shown in Fig. 5(a) in which an initial period of extension (<1% strain) exhibits relatively little strain hardening as the martensite forms, such as in NiTi.[18] It

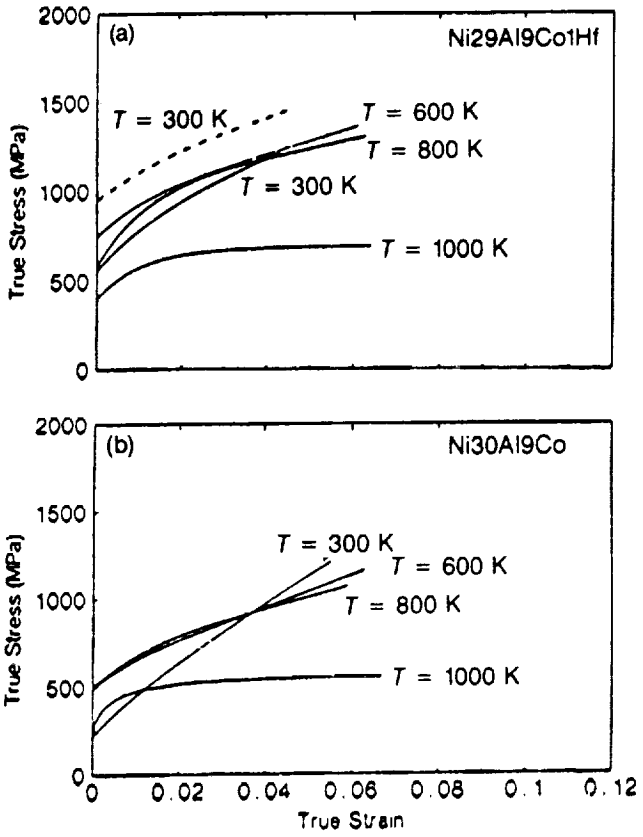

FIG. 6. True stress–true strain behavior of the blocky/irregular gamma-prime alloys: (a) Ni29Al1Co1Hf and (b) Ni20Al10Co. The specimens were in the hot-pressed condition except for the dotted line data in (a) which was for an as-extruded specimen.

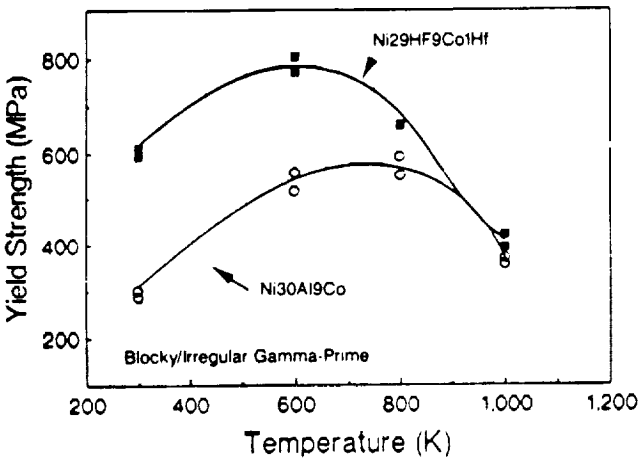

FIG. 7. The temperature dependence of the 0.2% offset yield stress for (a) the necklace γ' alloys and (b) the blocky irregular γ' alloys in the hot-pressed condition.

should be noted that at 5% strain this microstructure contains numerous intergranular microcracks due to incompatibility and barreling stresses which develop during compression. In some regions, grains have been "ejected" from the surface during deformation, which is consistent with the brittle behavior of the fully martensitic structures observed in ribbon testing.

While strain-induced martensite formation during deformation clearly has a significant influence in the stress-strain response, the strain-hardening rate of the martensite also appears to be somewhat higher than that of the B2 structure, at least at 600 K. This can be inferred by noting that the M_s of the Ni31Al18Co alloy should be about 750 K while that of the Ni35Al9Co alloy should be about 400 K.[14] With regard to strain hardening, we note that there is little difference in the magnitude of $d\sigma/d\epsilon$ ($d\sigma/d\epsilon \simeq 1.2 \times 10^4$ MPa for $0.02 \leq \epsilon \leq 0.04$) between 300 and 600 K in the (martensitic + γ')Ni31Al18Co alloy, but the strain hardening of the Ni35Al9Co decreases from $d\sigma/d\epsilon = 2.2 \times 10^4$ MPa at 300 K to 1.2×10^4 MPa at 600 K, at which temperature the martensite should have reverted to the B2 structure. This implies that $d\sigma/d\epsilon$ of the martensite is nearly twice that of the B2 structure at 600 K. We also note that the stress-strain responses of the Ni31Al18Co and Ni35Al9Co are very similar at 600 K with both having values of $d\sigma/d\epsilon \leq 1.2 \times 10^4$ MPa. Given that the M_s temperatures of these two alloys are 165 and 400 K, respectively, and in view of the typical temperature increments for heating transformations,[13] both of these alloys should have microstructures consisting predominantly of B2 structure. Thus, the data also are consistent with a lower strain-hardening rate of the B2, at least in the 600 K range. The higher rate of strain hardening of the martensite is also consistent with the behavior of single crystal Ni-36Al after an initial extension due to reorientation of martensite variants and is not surprising in view of the internally twinned structure of the martensite.[18]

The fracture behavior of the ribbon specimens suggests that the presence and location of the γ' phase has a strong effect on microcracking susceptibility. Examples of the range of microstructures are shown in Fig. 1, which depicts the Ni31Al18Co alloy heat-treated to a range of γ' contents. Specifically, a fully martensitic structure, Fig. 1(b), exhibits extensive intergranular microcracking while that containing approximately 19 vol.% γ', Fig. 1(a), is susceptible to occasional intergranular cracking along gamma-prime/martensite interfaces. In the latter case, the crack path was always along the interface, never within the γ' except to cross over to the other interface; note the microcrack denoted by an arrow in Fig. 1(a). The microstructure in Fig. 1(c), which contains about 33 vol.% γ' and a B2 structured matrix, shows no signs of microcracking. This no doubt reflects the increased volume fraction of γ'; the fact that the matrix is ordered bcc as opposed to martensite may also be a factor. It should also be noted that in ribbon form, this alloy was ductile with microstructures similar to Figs. 6(b) and 6(c).

In view of the above, we conclude that the presence of the γ' phase can be beneficial to ductility. Specifically, a thick ($\gtrsim 5$ μm) continuous film or necklace of γ' increases the resistance to strain-induced microcracking and thus should impart at least limited ductility in NiAl-based alloys. This is not surprising, given the well-known inability of $\langle 001 \rangle$ slip in the B2 NiAl alloys to satisfy grain boundary compatibility requirements; the thin film of γ' with its multiple $\langle 110 \rangle \{111\}$ slip systems can effectively act as a compliant layer within which grain-to-grain compatibility is restored. Thus, provided it is located such that it separates B2 or martensitic grains, the γ' phase can act as a compliant layer, and ductility will be imparted so long as interface fracture between the γ' and the matrix is inhibited.

3. Extruded material

Processing by extrusion provided enough material to obtain a few specimens for tensile testing. In the as-extruded condition, Ni31Al18Co is quite brittle, having a fracture strength of 525 MPa. In compression, this alloy in the extruded form exhibits a yield strength of 1006 MPa, which results in tensile fracture before plastic yielding occurs. Surprisingly, the as-extruded flow stress is much higher than the value of 430 MPa obtained in the hot-pressed condition, apparently the result of differences in residual dislocation content, γ' content and morphology, and texture. The as-extruded microstructure of this alloy consists of a martensitic matrix with a thin discontinuous γ' film, Fig. 4(a), and cracks tended to be initiated along those grain boundaries separating adjacent martensite grains which have little or no γ' present. After annealing for 96 h at 1073 K, the alloy possessed the microstructure shown in Fig. 4(b), with thick, continuous grain boundary γ'. This microstructure produced a fracture strength of 900 MPa and about 0.5% plasticity, and failed along γ'/β interfaces. This result is consistent with the earlier conclusion that the presence of a continuous film of γ' separating β grains can be beneficial for ductility, because the γ' phase can act as a compliant layer.

Compression testing of the two alloys with the blocky/irregular γ' microstructures after hot pressing indicated no sign of microcracking after 5% strain. This suggests that these alloys should be ductile in tension in bulk form. To test this possibility the Ni29Al9Co1Hf was hot extruded and specimens were tested in tension. Unfortunately, extrusion increased the compressive yield stress to 990 MPa, which is well above the tensile fracture stress of 810 MPa, and ductility was thus precluded by fracture. The microstructure shown in Fig. 2(a) could not be duplicated after extrusion or after subsequent heat treatments, as much of the γ' was nonuniformly distributed such that many martensitic grains were adjacent to each other. As a result, none of the specimens exhibited more than 0.3% room temperature ductility as microcracks readily initiated along those "martensitic" grain boundaries devoid of γ' phase.

IV. SUMMARY

The most significant result of this study is the observation that the presence of a continuous grain boundary film or "necklace" of the γ' phase can impart resistance to microcracking and at least some tensile ductility in otherwise brittle NiAl-based alloys. These observations are not surprising in view of the well-known inability of $\langle 001 \rangle$ slip within B2 NiAl alloys to satisfy grain boundary compatibility requirements during plastic deformation. As a result, the presence of a γ' film with its multiple $\langle 110 \rangle \{111\}$ slip systems enables grain-to-grain compatibility to be restored. In short, the gamma-prime acts as a "compliant layer" between normally incompatible adjacent deforming grains, as long as γ'/β interfacial fracture does not occur.

While the necklace-type morphology provides a good example of the compliant phase concept, other morphologies may also serve to relax the incompatibilities caused by an inadequate number of slip systems in NiAl structures at low temperatures. For example, a "blocky" gamma-prime microstructure is likely to be ductile as long as grains of the β phase or martensite are not adjacent to each other.

The presence of even 10% γ' phase also influences the other aspects of flow behavior of a NiAl-based alloy. In particular, the temperature dependence of the yield stress reflects the presence of the γ' phase. The results also suggest that, at the same composition, $L1_0$ martensite strain hardens about a factor of two more rapidly than its B2 counterpart in NiAl-based alloys, which appears to be related to the internally twinned structure of the martensite.

ACKNOWLEDGMENT

This research was supported by the NASA-Lewis Research Center through Grant No. NAG 3-827.

REFERENCES

[1] A.G. Rozner and R.J. Wasilewski, J. of Inst. of Metals **94**, 169 (1966).
[2] R.T. Pascoe and C.W.A. Newey, Met. Sci. **2**, 138 (1968).
[3] A. Ball and R. Smallman, Acta Metall. **14**, 1349 (1966).
[4] K.H. Hahn and K. Vedula, in *High Temperature Ordered Intermetallic Alloys III*, edited by C.C. Koch, C.T. Liu, N.S. Stoloff, and A.I. Taub (MRS, Pittsburgh, PA, 1989), p. 299.
[5] D.J. Gaydosh, R.W. Jech, and R.H. Titran, J. Mater. Sci. Lett. **4**, 138 (1985).
[6] S. Guha, P. Monroe, and I. Baker, Scripta Metall. **23**, 897 (1989).

[7]K.C. Russell and J.W. Edington, Metal Science Journal **6**, 20 (1972).
[8]A. Inoue, T. Masumoto, and H. Tomioka, J. Mater. Sci. **19**, 31097 (1984).
[9]C.C. Law and M.J. Blackburn, Air Force Report No. AFWAL-TR-87-4102, 1987.
[10]D.R. Pank, M.V. Nathal, and D.A. Koss, to be published in *High Temperature Ordered Intermetallics III*, edited by C.C. Koch, C.T. Liu, N.S. Stoloff, and A.I. Taub (MRS, Pittsburgh, PA, 1989), p. 561.
[11]D.J. Gaydosh and M.J. Crimp, in *High Temperature Ordered Intermetallic Alloys III*, edited by C. Koch, C.T. Liu, and N.S. Stoloff (MRS, Pittsburgh, PA, 1985), p. 429.
[12]M.F. Singleton, J.L. Murray, and P. Nash, in *Binary Alloy Phase Diagrams I*, edited by T.B. Massalski (ASM, Metals Park, OH, 1986), p. 12.
[13]V.S. Litvinov and A.A. Arkhangelskaya, Phys. Met. Metall. **44**, 131 (1978).
[14]S.M. Russell and M.J. Blackburn, in *High Temperature Ordered Intermetallic Alloys III* (Proc. Mater. Res. Soc. Symp.), edited by C.T. Liu, A.I. Taub, N.S. Stoloff, and C.C. Koch (Materials Research Society, Pittsburgh, PA, 1989), Vol. 133, p. 627.
[15]I. Locci, NASA Lewis Research Center, Cleveland, OH, 1989 (unpublished research).
[16]Y. Mishma, S. Ochiai, M. Yodogawa, and T. Suzuki, Trans. Jpn. Inst. of Metals **27**, 41 (1986).
[17]E.M. Schulson, I. Baker, and H.J. Frost, in *High Temperature Ordered Intermetallic Alloys II* (Proc. Mater. Res. Soc. Symp.), edited by N.S. Stoloff, C.C. Koch, C.T. Liu, and O. Izumi (Materials Research Society, Pittsburgh, PA, 1987), Vol. 81, p. 195.
[18]K. Enami, V.V. Martynov, T. Tomie, L.G. Khandros, and S. Nenno, Trans. Jpn. Inst. of Metals **22**, 357 (1981).

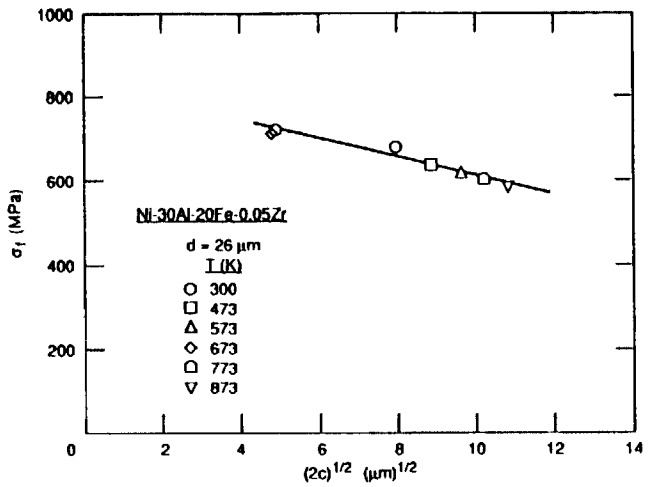

Figure 4. Plot of fracture stress against the square root of the defect size in accordance with linear elastic fracture mechanics.

REFERENCES

1. G. W. Groves and A. Kelly, Phil. Mag. 8, 877 (1963).
2. C. C. Law and M. J. Blackburn, Rapidly Solidified Lightweight Durable Disk Material, Final Technical Report, AFWAL-TR-87-4102.
3. D. B. Miracle, S. Russel and C. C. Law, in High-Temperature Ordered Intermetallic Alloys III, edited by C. T. Liu, A. I. Taub, N. S. Stoloff and C. C. Koch (Mater. Res. Soc. Proc. 133, Pittsburgh, PA 1989) p. 225.
4. A. Inoue, T. Masumoto and H. Tomioka, J. Mater. Sci. 19, 3097 (1984).
5. S. Guha, P. R. Munroe and I. Baker in High-Temperature Ordered Intermetallic Alloys III, edited by C. T. Liu, A. I. Taub, N. S. Stoloff and C. C. Koch (Mater. Res. Soc. Proc. 133, Pittsburgh, PA 1989) p. 633.
6. S. Guha, P. M. Guha and I. Baker, Scripta Metall. 23, 897 (1989).
7. S. C. Huang, R. D. Field and D. D. Krueger, Metall. Trans. 21 A, 959 (1990).
8. M. Larsen, A. Misra, S. Hartfield-Wunsch, R. Noebe and R. Gibala in Intermetallic Matrix Composites, edited by D. L. Anton, P. L. Martin, D. B. Miracle and R. McMeeking, (Mater. Res. Soc. Proc. 194, Pittsburgh, PA 1990) p. 191.
9. R. D. Noebe, private communication.
10. C. R. Barrett, Oxid. Met. 30, 361 (1988).
11. S. V. Raj, R. D. Noebe and R. Bowman, Scripta Metall. 23, 2049 (1989).
12. I. N. Sneddon, Proc. Roy. Soc. (Lond.) 187 A, 229 (1946).
13. S. Reuss and H. Vehoff, Scripta Metall. 24, 1021 (1990).

ON IMPROVING THE FRACTURE TOUGHNESS OF A NiAl-BASED ALLOY BY MECHANICAL ALLOYING

J. KOSTRUBANIC*, D.A. KOSS*, I.E. LOCCI+, AND M. NATHAL+

*Dept. of Mat. Sci. & Eng., Penn State University, University Park, PA 16802

+NASA Lewis Research Center, Cleveland, OH 44135

ABSTRACT

Mechanical alloying (MA) has been used to process the NiAl-based alloy Ni-35Al-20Fe such that a fine-grain (~2 µm) microstructure is obtained through the addition of 2 v/o Y_2O_3 particles. When compared to a conventionally processed, coarse-grained (~28 µm) Ni-35-20 alloy without the Y_2O_3 particles, the MA alloy exhibits two to three times higher fracture toughness values, despite a 50% increase in yield strength. Room temperature K_Q values as high as 34 MPa $\sqrt{m}$ are observed accompanied by a yield strength in excess of 1100 MPa. Fractography confirms a change in fracture characteristics of the fine-grained MA alloy.

INTRODUCTION

The issue to the poor ductility of NiAl alloys at room temperature is well known and has recently discussed in several reviews [1-3]. If the dependence of the yield stress on grain size is less than that of the fracture stress, a particularly attractive approach to improving ductility is grain refinement [5]. These fine-grain NiAl alloys should be ductile at room temperature if the grain size is sufficiently small. For grains smaller than the critical size, it has been hypothesized that the stress to nucleate grain-sized micro-cracks is less than that to propagate them, thus requiring work hardening and plastic deformation [4]. This hypothesis has been recently supported by a fracture-mechanics based analysis of the instability of grain-sized cracks propagating in a material whose toughness is independent of grain size [6].

Based on the above studies, estimates of the "critical" grain size in equiatomic NiAl range from < 1µm [6] to ~ 4 µm [3] in order for room temperature ductility to be achieved. An obvious difficulty with the above approach is the achievement of such fine grain sizes. Typically, the finest grain sizes for extruded binary NiAl are roughly 8-15 µm; and these specimens are usually brittle at room temperature [7,8]. Finer grain sizes have been achieved by ternary additions such as B, Zr, and Re but, if anything, these alloys have a higher ductile to brittle transition temperature than equiatomic NiAl [9].

The use of mechanical alloying MA to process metal containing oxide dispersoids is well known [10]. Of pertinance to this study is that MA alloys usually possess very fine grain sizes after powder consolidation; thus, MA presents an attractive processing route to obtain a fine-grain material. The problem with the application of MA to NiAl alloys is that the MA process requires a balance of cold welding of powder particles combined with concurrent fracture of agglomerated, cold-welded particles. Previous attempts to mechanically alloy NiAl with dispersoids were unsuccessful [11]. The brittle nature of NiAl powders resulted in powder grinding but insufficient cold welding, which requires ductility, to incorporate the dispersoid particles within a NiAl matrix. Perhaps the best "success" at MA of NiAl has been the "cryomilling" of NiAl in which nitrogen is introduced during the MA process; the result is improved creep strength but the room temperature mechanical properties are unknown [12].

The present investigation relies on the inherent ductility of melt-spun ribbons of the NiAl-based alloy Ni-35Al-20Fe to utilize MA successfully. Both fracture toughness and yield strength results are presented for hot-pressed, fully dense specimens which are characterized by (1) a fine, equiaxed grain structure with grain sizes of ~2 µm and (2) a fine-scale dispersion of sub-micron Y_2O_3 particles. Of particular significance is that, the consolidated, MA material, which has a B2 matrix, exhibits much higher fracture toughness values compared to either the conventionally processed Ni-35-20 alloy or a much softer equiatomic NiAl alloy.

Mat. Res. Soc. Symp. Proc. Vol. 213. © 1991 Materials Research Society

EXPERIMENTAL

The materials used in this study were based on prealloyed Ni-35Al-20Fe (at. %) ribbons produced by melt spinning and chopped into flakes ≤ 200 μm. In the case of the MA material, 2 v/o Y_2O_3 was added in the form of agglomerates of sizes of less than 10μm. Ball milling of the Y_2O_3-containing alloy was performed in a SPEX mill with a mass to charge ratio of 18:1. The cannister was charged in a glove box under high purity argon and subjected to 2 hours of ball milling. Other experimental details are described elsewhere [13].

Both the Y_2O_3-containing MA powder (hereafter denoted Ni-35-20 + Y_2O_3) and the Y_2O_3-free ribbon (Ni-35-20) were consolidated by hot-pressing at 1250°C for 4 hours at 35 MPa (MPa). Subsequently, these materials were also hot isostatic pressed at 1000°C and 140 MPA for 3 hrs. The chemical compositions of the consolidated material is indicated in Table I. The high values of C and O in the Ni-35-20 are caused by contamination during ribbon crushing.

Table I. Chemical Compositions of Consolidated Materials in wt %.

Material	Ni	Al	Fe	Y	C	O	S
Ni-35-20	56.6	19.4	23.8	--	.103	.17	.001
Ni-35-20+Y_2O_3	54.9	20.1	24.0	1.0	.037	.58	<.001

Mechanical tests were performed in compression to determine the stress-strain response and on notched bend bars to determine the fracture toughness values. Compression test specimens had a 3.4 mm square cross section and were 5.3 mm high. An initial strain rate of $2x10^{-4}$ s^{-1} was employed. Fracture toughness tests, which were based on sub-sized specimen geometries described elsewhere [14], consisted of four-point bend specimens 3.95 x 3.95 x 25.4 mm with a 1.3 mm deep notch which had a 125 μm tip opening radius. The notch was introduced by cutting with a thin-blade diamond saw. The lower and upper roll distances in the four-point bend apparatus were 20 and 10 mm respectively. A crosshead deflection rate of 0.5 mm/min was employed, and fracture toughness K_Q values were determined from critical loads according to ASTM Standard E399 for bend specimens. All tests were conducted in air at room temperature. It should be noted that data on a TiAl alloy indicate that a precracknd test specimen yields K_Q values about 20% lower than those obtained from specimens with notches of similar geometries to those used in this study [14].

RESULTS AND DISCUSSION

1. Microstructure

The Ni-35-20 alloy consists of equiaxed grains of roughly 28 μm; this is shown in Fig. 1a. As will be described elsewhere [13], this alloy may be quenched from ~ 1000°C to a single phase B2 structure, but it is susceptible to an age-hardening reaction in the 500-600°C range. As suggested by the Ni-Al-Fe phase diagram [15], age hardening appears to be due to the formation of ferromagnetic, Fe-rich precipitates, which have been observed at grain boundaries using TEM [13]. In view of the susceptibility to age hardening, the present study examines the Ni-35-20 in two heat-treat conditions: (1) a solution-treated condition (1000°C/2 hr + H_2O quench) denoted as ST and (2) a solution-treated and aged condition STA in which an additional 550°C/1 hr aging treatment is employed. The diamond pyramid hardness values (100 gm load) increase from ~320 kg/mm^2 in the ST condition to ~ 385 kg/mm^2 in the STA condition.

As shown in Figs. 1b, the Ni-35-20+Y_2O_3 alloy is characterized by a predominance of very small grains (~ 2 μm) surrounding an occasional large grain (~ 8-10 μm). Barely visible in Fig. 1b is a fine-scale, uniformly dispersed particle distribution which has pinned most grain boundaries such that ~ 90% of the microstructure consists of ~ 2 μm grains. The few larger grains have either grown during the 1250°C hot pressing or did not undergo MA during the

2 hour ball milling. As in the case of the Ni-35-20 alloy without the Y_2O_3 particles the Ni-35-20+Y_2O_3 is also susceptible to age hardening and was tested in the same heat-treat conditions as

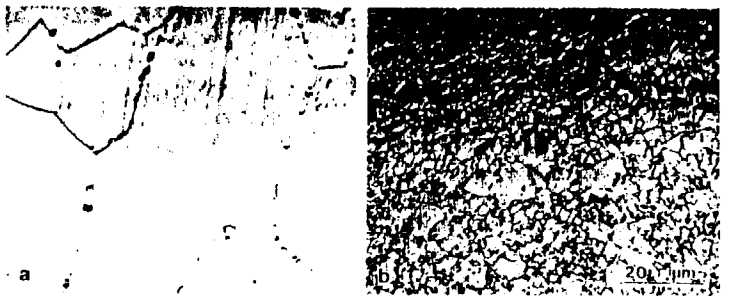

Fig. 1. Optical micrographs of (a) Ni-35Al-20 Fe and (b) mechanically alloyed Ni-35Al-20 Fe + v/o Y_2O_3.

the Ni-35-20: (1) ST and (2) STA. The diamond pyramid hardnesses increase from ~ 390 kg/mm in the ST conditon to ~ 425 kg/mm^2 in the STA condition.

2. Stress-Strain Response

The room temperature compressive stress-strain responses of both materials in both heat-treat conditions is shown in Fig. 2. Several trends are evident. First, when the data in Fig. 2 are compared to near equiatomic NiAl, the Ni-35-20 alloy has a much higher yield strength even in the solution-treated condition (~650 MPa vs ~ 250 MPa [7]). Secondly, age-hardening increases the yield stress by about 150 MPa and the flow stress at $\epsilon \geq 0.02$ by 250 MPa. This is consistent with the observed formation of Fe-rich precipitates upon aging at 550°C [13].

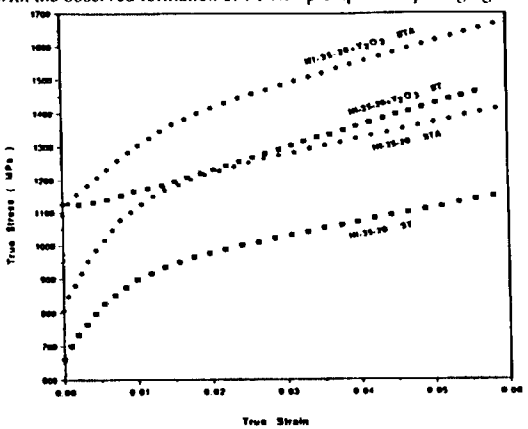

Fig. 2. True stress-true strain of Ni-35-20 and Ni-35-20 + Y_2O_3 as measured in compression.

Thirdly, the MA Ni-35-20+Y_2O_3 is considerably harder than Ni-35-20, exhibiting yield stresses in the 1150-1200 MPa range. This is no doubt partly a result of the order of magnitude finer grain size of the Y_2O_3-containing alloy as well as perhaps a small degree of particle hardening due to the small interparticle spacings of Y_2O_3 particles. Fourth, in all cases a high rate of strain hardening $d\sigma/d\epsilon \cong G/15$ is observed in the range $.02 \leq \epsilon \leq .06$ where microcracking is minimal (G, the shear modulus, is estimated from the modulus of NiAl at 72 GPa [16]). This is similar to the high rates of strain hardening which have been observed for near-equiatomic polycrystalline NiAl alloys at room temperature [7].

3. Fracture Toughness Behavior: Observations

The most significant result of this study is the high values of fracture toughness observed in the MA Ni-35-20 + Y_2O_3 alloys. Fig. 3 shows typically load-displacement responses of the Ni-35-20 as well as the Ni-35-20 + Y_2O_3 alloy. It is obvious that the MA alloy is not only much tougher but also exhibits a well-defined linearly elastic load-deflection response up to the failure load. In contrast, the Ni-35-20 specimens in both ST and STA conditions shows a non-linear load-displacement response, suggesting some stable crack growth occurs after initiation. In order to calculate a fracture toughness value for the Ni-35-20, we have chosen P_Q by drawing a line with a slope 5% less than the slope of the linear part of the load-displacement curve, as is done in conventional fracture toughness testing. The resulting K_Q may be viewed as an upper limit estimate of the fracture toughness. In the case of the MA Y_2O_3-containing

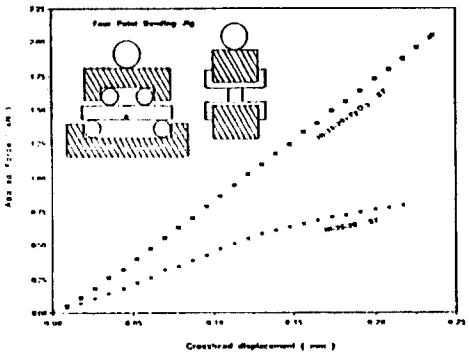

Fig. 3. Load-displacement data for notched bend specimens Ni-35-20 and Ni-35-20 + Y_2O_3.

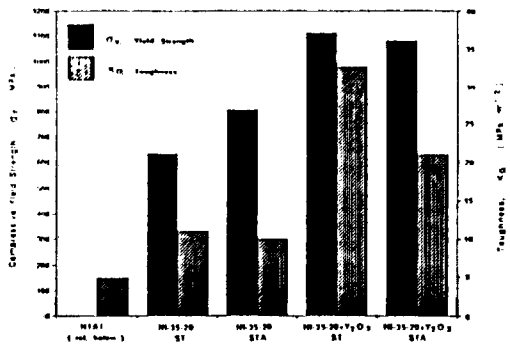

Fig. 4. Fracture toughness and yield stress values for the Ni-35-20 and Ni-35-20 + Y_2O_3 specimens in either the solution-treated ST or solution-treated-and-aged STA conditions. The NiAl data are from ref. 14.

alloy, no such ambiguity exists and P_Q corresponds to the maximum load attained during the linear load-displacement response.

Fig. 4 indicates that the fracture toughness values of the Ni-35-20 ($K_Q \equiv 9$-11 MPa $\sqrt{m}$) represent a definite improvement over those (5 MPa $\sqrt{m}$) obtained for equiatomic NiAl [17]. This is very likely due in part at least by the coarse grain size of 200-500μm of the NiAl as compared to 28 μm for the Ni-35-20. It might be noted that in the NiAl fracture toughness tests, a much slower crosshead speed (12 μm/min) and blunter notch (150 μm radius) was employed [17]. Both of these effects may increase the apparent toughness.

Fig. 4 also shows the most significant observation of the present study: the high fracture toughness of ~ 34 MPa $\sqrt{m}$ determined for the solution-treated Ni-35-20 + Y_2O_3 alloy. This value is three times that of conventionally processed Ni-35-20 and six times greater than that reported for coarse-grain NiAl. While we recognize that the absence of a pre-crack inflates our toughness value, the data in Fig. 4 clearly indicate that a very significant increase in K_{IC} occurs in the MA material. This is true even in the age-hardened condition in which a toughness of ~23 MPa $\sqrt{m}$ is observed.

Careful examination fractography confirms that the MA material has different fracture characteristics than the conventional Ni-35-20. Immediately apparent in Fig. 5 are the differences in the scale of the features on the fracture surfaces of the Ni-35-20 as compared to the Ni-35-20 + Y_2O_3. Fig. 5a and b indicates that the "conventional" Ni-35-20 fractures by predominantly transgranular cleavage in both the solution-treated and the aged conditions. The aged material also contains intergranular facets wherein the crack propagated along the grain boundaries (see arrows in Fig. 5b).

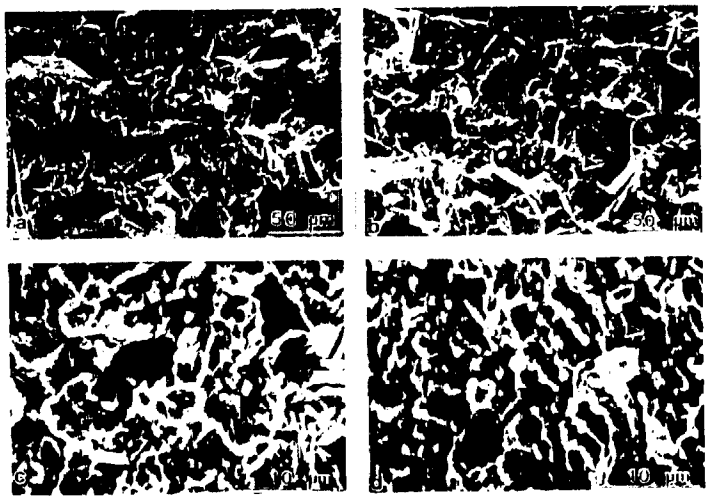

Fig. 5. Scanning electron micrographs showing the fracture surfaces of (a) Ni-35-20 in the ST condition, (b) Ni-35-20 in the ST condition, (b) Ni-35-20 in the STA condition, (c) Ni-35-20 + Y_2O_3 in the ST condition, and (d) Ni-35-20 + Y_2O_3 in the STA condition.

In contrast, as shown in Figs. 5c and d, the MA alloy shows a mixture of cleavage and very fine-scale, torturous "tearing" of the "ligaments" between cleavage facets. The ligaments clearly suggest localized plastic deformation is occurring. Most cleavage facets usually are 5-10 μm in size and only a few are in the 2 μm range. Thus, the coarse-grain areas tend to cleave while the fine-grained regions show evidence of ductility and considerable roughness. While the same cleavage "behavior" is also very evident in the aged version of the Ni-35-20 + Y_2O_3 alloy, there are also intergranular I/G fracture facets commonly present (see Fig. 5d). An

examination of many fractographs indicates that I/G fracture is confined to grains ≤ 5 μm. This is in contrast, to the cleavage of grains 5-10 μm is size which are common in both heat-treat versions of the MA alloy.

SUMMARY

The present study clearly indicates a strong grain size effect of fracture toughness in B2 NiAl-based alloys. The combination of a small amount of Y_2O_3 (2 v/o) particles plus an order of magnitude decrease in grain size increases the fracture toughness by a factor of three. This occurs despite a 50% increase in the room temperature yield strength to 1150-1200 MPa. Thus, both the strength and toughness have been significantly increased when compared to equiatomic NiAl. This suggests that ductility enhancement due to decreasing grain size probably cannot be analyzed simply in terms of the decreasing size of easily nucleated grain-size cracks propagating through material whose toughness is independent of grain size. Rather, as was suggested in a recent theoretical analysis of grain size on ductility [6], at sufficiently small grain sizes there appear to be very significant increases in fracture toughness. We believe that such behavior can be understood by a concept of a crack initiation stress which is itself very strongly grain-size dependent at small grain sizes. As a consequence, a material, such as the MA Ni-35-20 + Y_2O_3, which has a few large grains (~ 10 μm) dispersed in a matrix of fine grains (~ 2 μm) will exhibit high toughness due to the combination of (a) difficult crack initiation/growth across the small grains and (b) crack tortuosity caused by cleavage of the dispersed large grains. This hypothesis, a related physical model, and its implications to improved fracture toughness in NiAl alloys will be examined in more detail in a subsequent publication.

ACKNOWLEDGEMENT

This research has been supported by the NASA Lewis Research Center.

REFERENCES

1. R. D. Noebe, R. R. Bowman, J. T. Kim, M. Larsen, and R. Gibala in High Temperature Aluminides and Intermetallics (eds. S. H. Whang, C. T. Liu, D. P. Pope, and J. O. Stiegler), Warrendale, PA: TMS, 1990, p. 271.
2. K. Vedula nd P. S. Khadkikar, ibid, p. 197.
3. I. Baker and P. R. Munroe, ibid, p. 425.
4. E. M. Schulson: Res. Mech. Letters, 1, 1981, p. 111.
5. E. M. Schulson and D. R. Barker: Scripta Metall., 17, 1983, p. 519.
6. K. S. Chan: Scripta Metall., 24, 1990, p. 1725.
7. K. H. Hahn and K. Vedula: Scripta Metall., 23, 1989, p. 7.
8. R. R. Bowman, R. D. Noebe, and S. V. Raj, unpublished research.
9. R. D. Noebe, R. R. Bowman, C. L. Cullers, and S. V. Raj, Hi Temp Review 1990, 1990, p. 20-1.
10. P. S. Gilman and J. S. Benjamin: Ann. Rev. Mater. Sci., 1983, p. 279.
11. K. Vedula, G. M. Michal, and A. M. Figueredo, Modern Developments in Powder Metall. 20, 1988, p. 491.
12. J. D. Whittenberger, E. Arzt, and M. J. Luton, J. Mater. Res. 5, 1990, p. 271.
13. J. Kostrubanic, I. E. Locci, M. V. Nathal, and D. A. Koss: unpublished research.
14. K-M. Chang and D. A. Catharine, Tech. Report No. 90 CRD154, GE Research & Development Center, Aug. 1990.
15. A. J. Bradley: J. Iron Steel Inst., London, 168, 1951, p. 233.
16. J. R. Hellmann, D. A. Koss, C. A. Moose, R. R. Petrich, and M. N. Kallas: Hi Temp 1990, 1990, p. 41-1, NASA CP-10051.
17. S. Reuss and H. Vehoff: Scripta Metall. 24, 1990, p. 1021.

STRUCTURE/PROPERTY RELATIONSHIPS IN A RAPIDLY SOLIDIFIED AND ANNEALED TERNARY IRON ALUMINIDE

B. Décamps*, M.A. Gibson†, A.J. Morton† and A. Wolfenden‡
* CNRS, Métallurgie Structurale, BAt. 413,Université Paris-sud,91405, Orsay, France
† CSIRO, Div. of Materials Science and Technology, Clayton Vic. 3168, Australia
‡ Texas A&M University, Advanced Mats. Lab., College Station, TX 77843-3123, USA

ABSTRACT

Rapidly solidified strips of Fe66.5-Al28.5-Cr5 alloy with the addition of 0.5wt.% TiB_2 were produced by planar flow strip casting. Correlations of the microstructure and room temperature mechanical properties were made for strips in the as-cast condition and after annealing at 1273K for periods up to 4hrs. The results showed that grain size, tensile strength, ductility, hardness and Young's modulus were very stable for the times investigated. Studies of tensile fracture surfaces revealed essentially 100% transgranular cleavage in the as-cast strip with a greater tendency for intergranular failure after prolonged exposure to high temperatures. TEM studies of this alloy revealed diffraction patterns characteristic of DO_3 ordering but the dislocations observed in both as-cast and deformed specimens were those typical of the B2 structure without any extended APBs. This is attributed to the very fine DO_3 domain size . At room temperature <111> slip is predominant.

INTRODUCTION

As a class of engineering materials the ordered intermetallic alloys occupy an intermediate position between structural ceramics and the usual metallic alloys. It is this intermediate behaviour that provides both the promise and the difficulties associated with the use of intermetallics as structural materials. Intermetallic compounds based on aluminium have been shown to exhibit a number of desirable properties including high temperature strength, stiffness, oxidation resistance and low density [1,2]. Their major disadvantage, however, is limited ductility, particularly at room temperature [2].

Rapid solidification processing (RSP) has been used extensively during recent years [3] to enhance the strength and ductility of intermetallics through grain refinement and the introduction of a uniform distribution of stable fine particles throughout the microstructure. The work reported here is part of an extensive study of ternary iron aluminides which has been undertaken to determine the influence of composition and RSP on alloy microstructure and associated deformation mechanisms. This paper reports preliminary findings on the structural stability, mechanical properties and dislocation structure of Fe66.5-Al28.5-Cr5 + 0.5wt.% TiB_2 annealed at 1273K.

EXPERIMENTAL

Alloys were prepared by argon arc melting on a water cooled copper hearth of weighed quantities of Fe (99.95%), Al (99.93%), Cr (99.95%) and sufficient Al/Ti/B master alloy to produce an alloy containing 0.5wt.% TiB_2.

Rapidly solidified strip of thickness 70-120μm and width 8-10mm was produced from the ingots by planar flow casting using quartz crucibles (the quartz was isolated from the melt by a layer of colloidal graphite) onto a stainless steel wheel rotating with a peripheral velocity of 8.6 $msec^{-1}$.

Specimens for metallographic and TEM examination and for mechanical property measurements were prepared from strip in the as-cast condition and after annealing in argon at 1273K for periods of 1 and 4 hours. In general the

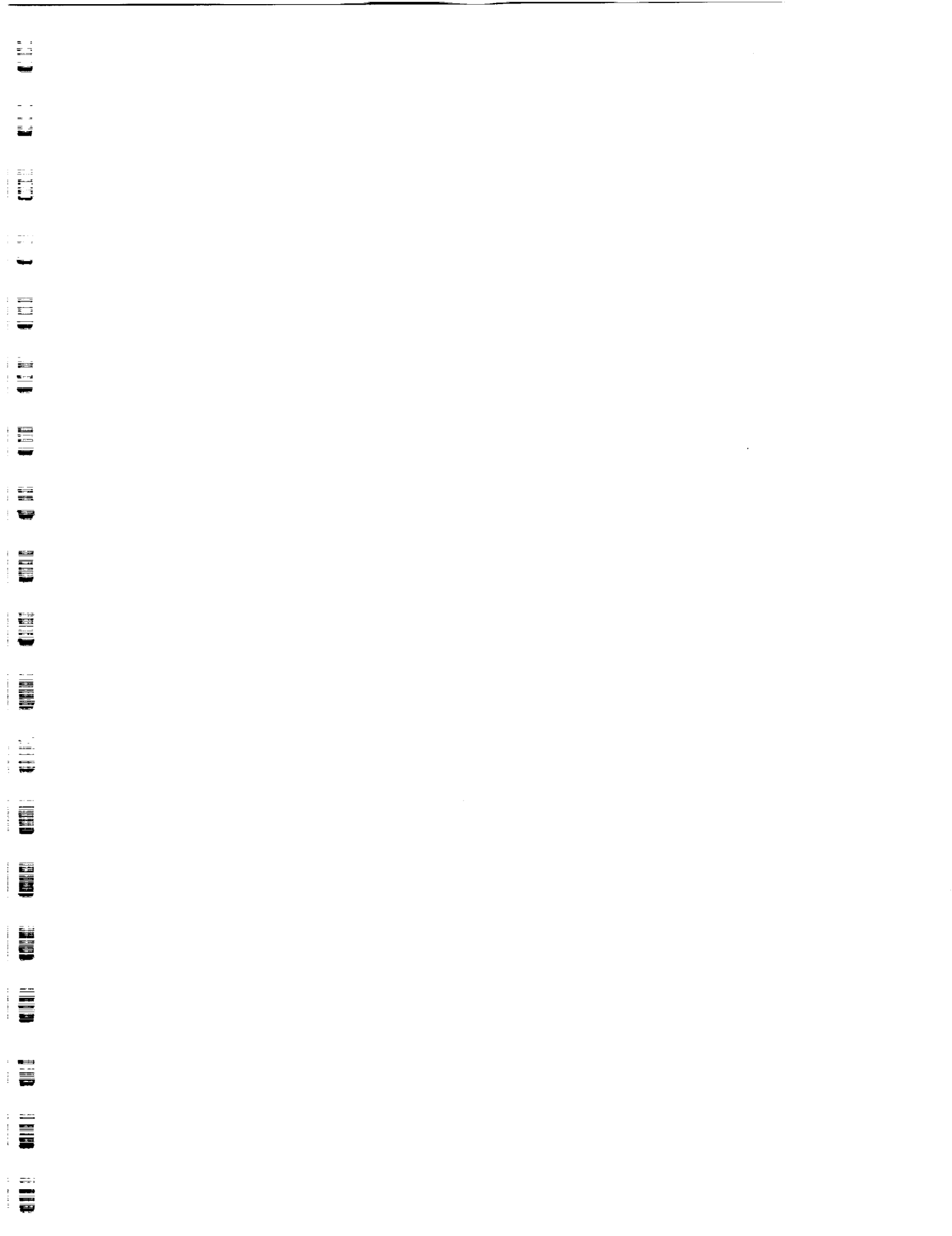

To be published in Int. Symposium on Structural Intermetallics

THE INFLUENCE OF PROCESSING AND THERMAL HISTORY ON THE PROPERTIES OF NiAl-BASED ALLOYS CONTAINING IRON

J. M. Kostrubanic, J. B. Breedis, D. A. Koss, I. Locci°, and J. M. Poole&

Department of Materials Science and Engineering
The Pennsylvania State University
University Park, PA 16802

° NASA-Lewis Research Center,
Cleveland, OH 44135

&Inco Alloys International
Huntington, WV 25720

Abstract

The influence of processing techniques and thermal history on the flow and fracture behavior of a series of B2 NiAl-Fe alloys was examined. Three compositions, Ni-35Al-20Fe, Ni-45Al-13Fe, and Ni-37Al-14Fe (compositions in atomic percent), were studied in melt-spun ribbon form. The Ni-35Al-20Fe and Ni-45Al-13Fe alloys are both susceptible to age hardening response due to the formation of Fe-rich precipitates during annealing between 500 to 750°C. Bend tests of ribbons indicate ductility in the Ni-35Al-12Fe and the Ni-35Al-20Fe alloys in the single phase B2 condition. Furthermore, cast and extruded counterparts of these two alloys exhibit room temperature ductility as well as enhanced fracture toughness (as high as 22 $MPa\sqrt{m}$). Two compositions, Ni-35Al-20Fe and Ni-31Al-15Fe, each containing one vol. pct. Y_2O_3, were also powder processed using mechanical alloying (MA) and consolidated by hot extrusion. Following grain coarsening anneals, tests show the MA-processed alloys exhibit both enhanced room temperature toughness ($K_{IC} \simeq 21$ $MPa\sqrt{m}$) and improved creep strength at 1000°C.

Introduction

As evidenced by two recent and extensive reviews [1,2], there has been a significant degree of interest in ordered intermetallic alloys based on the compound NiAl. The low density, high melting temperature, good thermal conductivity, and resistance to environmental degradation make NiAl and certain NiAl-based alloys very attractive for advanced aerospace applications. The major problem with these B2 alloys continues to be their poor fracture resistance at low temperatures combined with inadequate creep resistance at high temperatures. Both microalloying and macroalloying approaches have been attempted in order to alleviate the above problems. Small additions (<0.25 at. pct.) of Fe have been reported to impart room temperature ductility in <110> oriented single crystals [3] while large additions of Fe to melt-spun Ni-30Al-20Fe (at. pct.) wires also resulted in tensile ductility [4]. In addition, there is a report that Fe improves the creep resistance of NiAl + Fe alloys [5]. Enhanced room temperature toughness, based on notched specimens, has also been reported for a Ni-35Al-20Fe + 2 v/o Y_2O_3 alloy processed by mechanical alloying (MA) [6]. Despite the above, alloying additions to NiAl alloys usually increase their ductile to brittle transition temperature, and other researchers have been unsuccessful in their efforts to obtain room temperature ductility in the B2 intermetallic alloy Ni-30Al-20Fe + 0.5Zr [7-9].

The present study examines the room temperature fracture resistance of ribbons as well as bulk specimens of a series of macroalloyed NiAl + Fe alloys which retain the B2 intermetallic structure. We also briefly examine the microstructural stability of these alloys, particularly with respect to the possible formation of Fe-rich precipitates which can age-harden and embrittle the alloys. One focus of this study is to utilize the inherent ductility of these NiAl-Fe alloys to enable cold welding during MA as a means of processing oxide-dispersion strengthened NiAl-based alloys. Our effort differs in this respect from previous efforts in which MA processing techniques have been applied to brittle powders [10-13], wherein cold welding of powder particles to entrap oxide dispersoids does not occur. This study presents preliminary results of two alloys processed by MA: Ni-35Al-20Fe (at. pct.) and Ni-31Al-15Fe (at. pct.) each containing 1 vol. pct. Y_2O_3. Tests of the consolidated MA NiAl-based alloys indicated that improved values of room temperature fracture toughness are possible in elongated, coarse-grained microstructures which also appear to have promise for improved creep strength at elevated temperatures. This aspect of the present study complements a companion paper which focuses on the application of mechanical alloying to NiAl + Fe alloys [14].

Experimental Procedure

The present study is based on six B2 NiAl -Fe alloys with compositions and processing procedures listed in Table I. In all cases, the alloys will be designated by their Al and Fe contents, respectively [e.g.: Ni-35Al-20Fe will be designated Ni-35-20] and whether or not

Table I. Chemical compositions of alloys in at. pct.

Alloy	Form	Ni	Al	Fe	Y_2O_3†	C	O
Ni-35-20	ribbon	45.1	34.8	20.0	N/A	0.040	0.020
Ni-37-14	ribbon	48.5	37.5	13.6	N/A	0.380	0.033
Ni-45-13	ribbon	42.3	45.1	12.6	N/A	0.035	0.025
Ni-35-20	cast and extruded++	46.0	34.9	19.1	N/A	0.016	0.028
Ni-35-12	cast and extruded++	53.2	34.4	12.3	N/A	0.026	0.017
MA Ni-35-20	MA, extruded°	44.6	34.4	19.4	.82	0.140	1.451
MA Ni-31-15	MA, extruded°	51.9	31.2	14.8	1.05	0.096	0.765

†In vol. %.
++Cast and extruded at 920°C at a strain of 5.0.
°Hot extruded at 1186°C (MA Ni-35-20) and 1161°C (MA Ni-31-15) at strains of 3.1 (MA Ni-35-20) and 1.8 (MA Ni-31-15), respectively.

they were processed by MA [e.g.: Ni-35Al-20Fe + 1 vol pct Y_2O_3 processed by MA will be designated MA Ni-35-20]. The melt-spun ribbons were obtained by free-jet melt spinning onto a rotating copper wheel as described elsewhere [15]. The dimensions of the ribbons were typically 2-3 mm wide, 10-40 μm thick, and 2-3 cm long. Both microhardness (100 gm load) and bend tests were used to assess the mechanical properties of the ribbons. In the latter case, the fracture strain (elastic + plastic), e_f, is reported and was obtained by measuring the bend radius, r, at fracture and by calculating the total strain at the outer ribbon surface $e_f = t/(2r + t)$, where t is the ribbon thickness. For each condition, 8 to 10 tests were performed: half with the ribbon surface which contacted with copper wheel during solidification located on the inner bend radius and half on the outer bend radius. The ribbons initially were nearly flat. Data for specimens with the ribbon surface contacting the copper wheel tested in tension usually had 0.2-0.5% higher fracture strain values.

Since some of the alloys are susceptible to age hardening (due to the formation of Fe-rich disordered precipitates) at intermediate temperatures (i.e., 500-550°C), all alloys were solution treated at 1000°C for 1 hour and air cooled to produce a single phase B2 microstructure. The alloys in cast and extruded bar form as well as in ribbon form had grain sizes of ~40 to ~50 μm after the 1000°C heat treatment. The average grain size of both MA alloys after consolidation was about 2 μm. Grain coarsening of the MA materials at 1335°C for 1 hr resulted in elongated grains with a major dimension of ~800 μm and an aspect ratio of ~3 in the MA Ni-35-20 and MA Ni-31-15 alloys. Optical micrographs of the MA Ni-35-20 alloy, which are representative of the MA alloy microstructures, are shown in Figure 1.

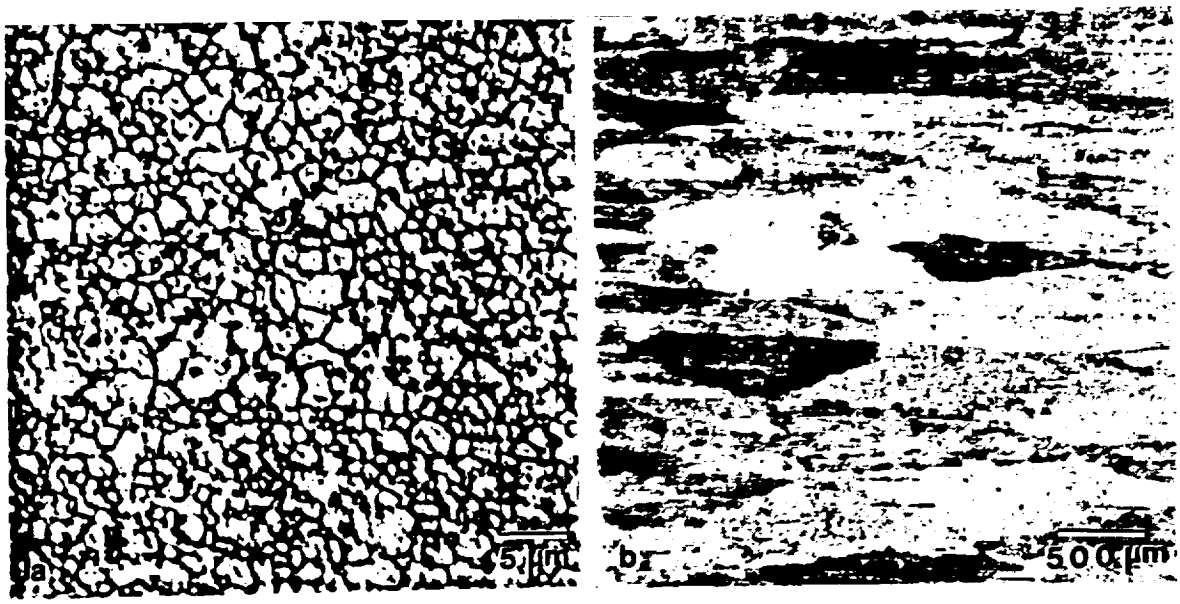

Figure 1. Optical micrographs of the MA Ni-35-20 alloy in the (a) fine-grained and (b) grain coarsened conditions.

In order to assess the degree of superparamagnetic behavior due to the formation of Fe-rich precipitates in the NiAl-Fe alloys, the following crude but effective technique was used. The number of 2 cm. sections of ribbons supported by a permanent magnet were examined for super-paramagnetic behavior as a function of heat treatment. A high degree of superparamagnetic behavior, indicative of a large amount of the Fe-rich phase, resulted in a large number of ribbons being attracted to the magnet. The relative degree of superparamagnetic behavior was confirmed by detailed magnetization measurements of the Ni-35-20 alloy in ribbon form as a function of external field using a Vibrating Sample Magnetetometer [15].

Fracture toughness tests were performed on short-rod chevron-notched specimens according to ASTM E-1304-89 [16]. The materials were tested such that crack growth occurred parallel to the axis of either the 19 mm diameter bar (MA materials) or the 12.7 mm diameter bar (cast and extruded Ni-35-20 and Ni-35-12 alloys). The toughness data is for material tested at room temperature in the single phase B2 condition after air cooling from 1000°C.

Tensile tests were performed at room temperature at an initial strain rate of $2x10^{-4}$ s^{-1} on specimens with a gauge length of 30 mm and a diameter of 3 mm. Slow strain-rate compression tests were performed at 1000°C in air to assess the steady state creep resistance of the MA materials. Tests were performed on 5.2 x 3.4 x 3.4 mm right-rectangular samples at strain rates from $2x10^{-5}$ s^{-1} to $2x10^{-2}$ s^{-1}.

Results and Discussion

A. Microstructural Characteristics

As shown in Fig. 2 [17], the Ni-Al-Fe alloys used in this study are located just within or near a two-phase field consisting of an ordered, intermetallic B2 NiAl-based phase (β) and a Fe-rich disordered bcc phase (α). Annealing the material at 1000°C and air cooling is sufficient to retain a B2 ordered structure in all of the alloys. This was confirmed by both x-ray diffraction and transmission electron microscopy, TEM. The absence of magnetic behavior as indicated by our measurements of the degree of superparamagnetic behavior also indicated the absence of the Fe-rich α phase.

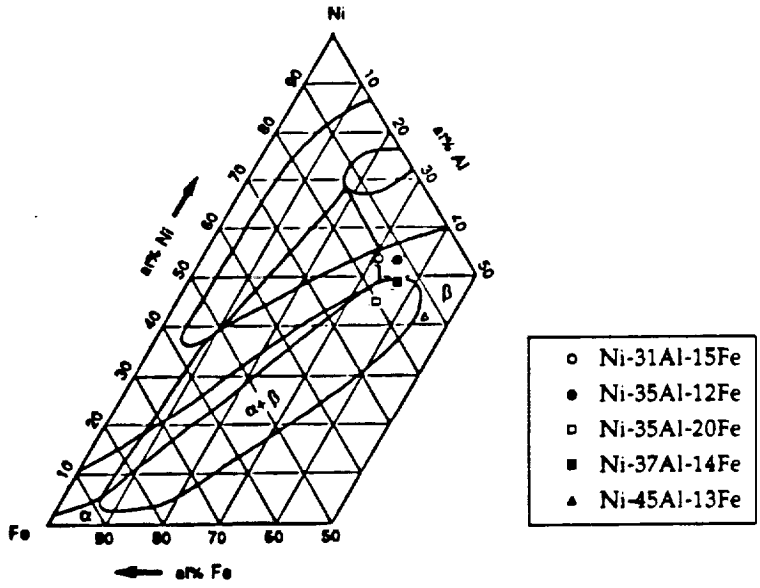

Figure 2. Isothermal section of the Ni-Al-Fe ternary phase diagram at 750°C showing the compositions of alloys examined [17].

In view of the alloy compositions in Fig. 2 [17], we expect that many of the alloys will be susceptible to the formation of bcc α-phase precipitates in the intermetallic (Ni,Fe) Al matrix upon annealing at or below 750°C. The precipitates result in an age hardening response of the Ni-45-13 and Ni-35-20 alloys as shown in Figure 3. Consistent with the age hardening, the degree of superparamagnetic behavior in Figure 4 indicates the formation of the α-phase in the Ni-45-13 and Ni-35-20 alloys. The age hardening response of the Ni-45-13 alloy at 550 and 650°C indicates that, at least at T < 650°C, the Ni-45-13 composition is located within the α+ β phase field in Fig. 2. Long term anneals (190 hrs) of the bulk Ni-35-12 alloy at 300°C confirm the absence of significant age hardening and no detectable superparamagnetic behavior of this alloy. This is supported by the behavior of the Ni-35-12 ribbons in Figures 3 and 4.

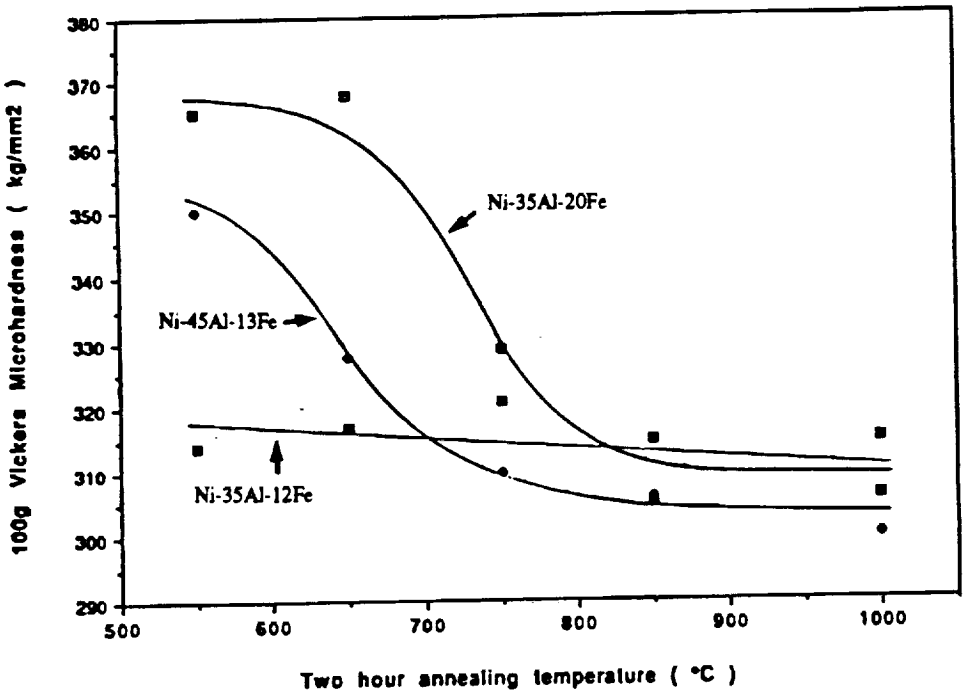

Figure 3. Microhardness values for NiAl-Fe specimens as a function of two-hour anneals at the temperatures indicated. All specimens were previously annealed at 1000°C and quenched.

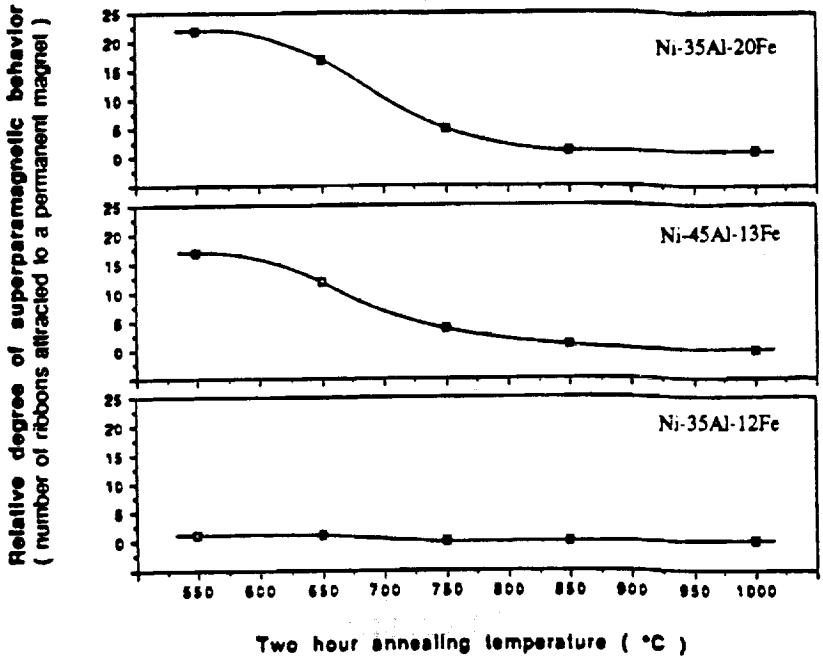

Figure 4. The relative degree of superparamagnetic behavior as a function of annealing temperature for NiAl-Fe alloys.

Thus we conclude that the Ni-35-12 alloy exhibits microstructural stability; the formation of Fe-rich α-phase precipitates, which can embrittle the alloy, does not appear to occur.

Consistent with the age hardening and magnetic measurements, transmission electron microscopy (TEM) performed on ribbon material, Figure 5a, shows the presence of a uniform dispersion of roughly spherical particles approximately 7 nm in diameter in a Ni-35-20 alloy

aged 130 hr at 550°C after a solution treatment at 1000°C. Energy dispersive analysis on the larger precipitates present on the grain boundaries confirms that they are Fe-rich (Figure 5b). At shorter aging times, a very fine modulated microstructure is evident within the grains. Both the particle shape and the fine-scale, uniform distribution suggest a high degree of lattice match between the bcc Fe-based particles and B2 NiAl-based matrix in the Ni-35-20 alloy.

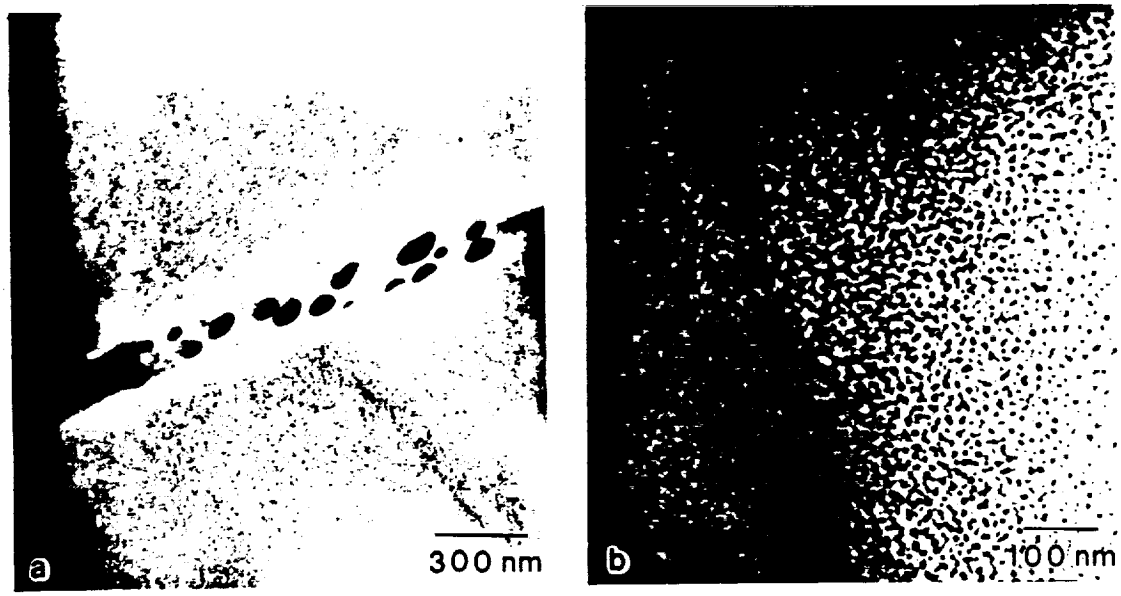

Figure 5. Transmission electron micrographs of the melt-spun ribbons of the Ni-35Al-20Fe alloy solution treated at 1000°C for one hour, quenched, and aged at 550°C for (a) 130 hours and (b) 16 hours.

B. Bend Ductility of Ribbon Materials

Based on our bend tests of the NiAl-Fe alloys in ribbon form, Figure 6 confirms the presence of room temperature ductility in both the Ni-35-20 and Ni-35-12 alloys. Except for a trace of plasticity (permanent bend before fracture) in some of the Ni-45-13 alloy specimens after quenching from 1000°C, this alloy behaved in a brittle manner after subsequent, lower temperature anneals. In contrast, if roughly 2% outer fiber strain is elastic at fracture, the Ni-35-20 ribbons exhibited ≈3% to 4% plastic strain to failure after anneals at 750°C, 850°C and 1000°C (grain size $\simeq$ 40μm $\simeq$ ribbon thickness). Despite the attractive bend ductility after cooling from T $\geq$ 750°C, the Ni-35-20 alloy embrittled after exposure at 550°C, presumably due to the Fe-rich precipitates which form as described previously. In contrast, the bend plasticity prior to failure of the Ni-35-12 alloy specimens remains finite ($e_f \simeq 1$ to 2% plastic strain), and is resistant to embrittlement by annealing. This is consistent with the resistance of this alloy to the formation of the Fe-rich, α phase.

Brittle, polycrystalline NiAl alloys usually fail at room temperature by intergranular fracture [1]. In the present study, failure in all three alloys occurs predominantly by cleavage. The exception is the brittle Ni-35-20 alloy which fractures by intergranular fracture mixed with cleavage after annealing at T $\leq$ 650°C. The loss of ductility and change in fracture mode is probably related to the Fe-rich grain boundary precipitates which form during aging; see Figure 5b.

It is useful to compare our "ribbon" results with those of Inoue et al [4] for wires made by in-rotating-water rapid solidification of a Ni-30Al-20Fe alloy. Those wire specimens were single phase, had a B2 structure, 4 μm grain size but a specimen diameter >80μm, and displayed 5% elongation characterized by dimple and intergranular fracture. In the present case, the Ni-35-20 ribbons also exhibit significant ductility (≈3% to 4% plastic strain in bending), provided that a single phase B2 structure was retained. The B2 Ni-35Al-12Fe alloy also exhibits ductility of

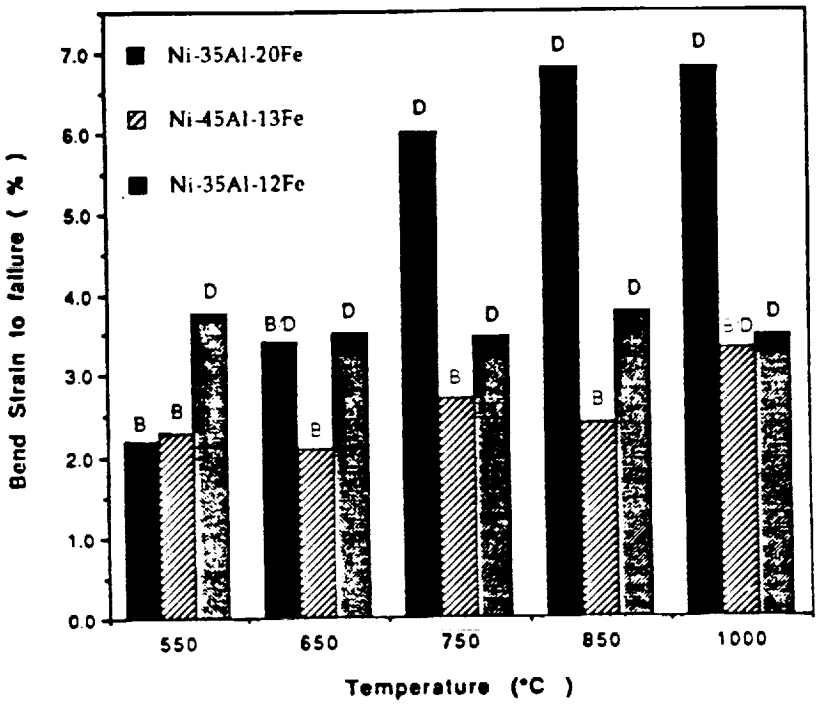

Figure 6. The bend strain to failure for NiAl-Fe ribbons as a function of annealing temperature. All specimens were solution treated at 1000°C for 1 hour and quenched prior to annealing and the data are averages of eight tests per condition. The letter B denotes brittle response while D denotes the presence of plastic deformation.

≈1-2% plastic strain. However, the grain sizes of our ribbon specimens were typically ≈40μm, or sufficiently large such that single grains extended through the thickness of the ribbon. Thus, there is question in our case as to whether or not the results of our ribbon specimens represent polycrystalline or single crystal ductility.

C. Fracture of Bulk Materials: Cast and Extruded NiAl + Fe Alloys

The presence of bend ductility in rapidly solidified NiAl + Fe wires or ribbons suggests that the bulk material may also be ductile at room temperature. Published results for a similar bulk alloy, polycrystalline Ni-30Al-20Fe, are mixed. While tensile tests of cast and double-extruded specimens with a grain sizes ~ 25 μm show 2.5% plastic strain [18], most investigators observe brittle behavior at room temperature of nearly identical compositions processed by hot extrusion of prealloyed powders [7-9].

At room temperature, the Ni-35-12 alloy (grain size = 45 μm) exhibited tensile ductility ranging from 1-2% plastic strain to failure; see Figure 7. In all cases fracture was initiated from either an internal flaw (~40 μm in size) or by surface initiation sites, which appear to be roughly 300 to 400 μm deep and 1.1 to 1.3 mm long at the onset of fast fracture. Tensile specimens of the Ni-35-20 alloy (grain size ~50 μm) show a tensile response ranging from brittle (prone to grip failure) to 1.8% plastic strain to failure. In the latter case, failures were initiated by an internal flaw (~100 μm to ~300 μm in size). Figure 7 shows the tensile stress-strain responses of the Ni-35-12 and Ni-35-20 alloys. While these specimens originated from cast and extruded material, it might be noted that the same alloy in hot-pressed form shows only ~0.5% bend ductility [15]. As in other NiAl alloys which possess room temperature ductility [1], the fracture surface is predominantly cleavage (Figure 7).

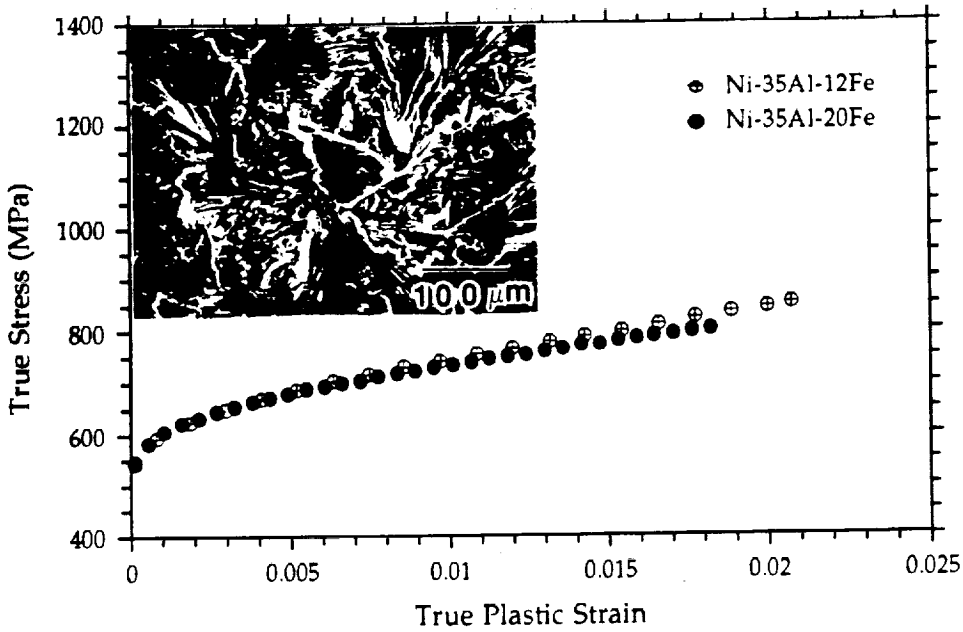

Figure 7. The room temperature tensile stress-stain response of cast-and-extruded Ni-35Al-12Fe (grain size ≈ 45μm) and Ni 35Al-20Fe (grain size ≈ 50μm). The insert shows the fracture surface and an inclusion which initiated failure in the Ni-35-20 specimens.

The presence of the inclusions in the cast NiAl-Fe alloys suggests, as Chan has analyzed for grain-size effects [19], that the ductility of NiAl alloys may be limited by the growth of a penny-shaped crack whose size is that of a grain (or in our case: an inclusion). The large size (40 to 100 μm) of the inclusions, or of the surface flaws, and high fracture stresses (~800 MPa) in Figure 7, suggest a fracture toughness much higher than the 4-6 MPa$\sqrt{m}$ value typical of equi-atomic, polycrystalline NiAl at room temperature [22,23]. In the next section, based on the internal "flaws" present on some of the fracture surfaces of our tensile specimens, we estimate a fracture toughness significantly higher (15-19 MPa $\sqrt{m}$) than equi-atomic NiAl; the subsequent section provides experimental data to support this expectation.

Using an analysis identical to Chan's for grain-size effects [19], we can estimate the fracture toughness of the two NiAl-Fe alloys in Figure 7 by assuming the inclusions act as internal circular cracks in a plastically deforming matrix. Extension of the cracks is dictated by a critical J-integral condition which, for a circular round bar at stress σ_∞ is [20]

$$J = J_e\,(1 + J_z/J_e + J_pJ_e) \tag{1}$$

where

$$J_e = 0.405\,(1-\nu^2)\,\sigma_\infty^2\,\pi a(E)^{-1} \tag{2}$$

$$\frac{J_z}{J_e} = 0.0675\,\left(\frac{N-1}{N+1}\right)\left(\frac{\sigma_\infty}{\sigma_y}\right)^2\left[1 + \left(\frac{\sigma_\infty}{\sigma_y}\right)^2\right]^{-1} \tag{3}$$

$$\frac{J_p}{J_e} = \frac{3}{2(1-\nu^2)\sqrt{1 + 3/N}}\left(\frac{\varepsilon^p}{\varepsilon_e}\right) \tag{4}$$

and

$$K = \sqrt{\frac{E\,J}{1 - \nu^2}} \qquad (5)$$

where $\nu \cong \frac{1}{3}$ is the Poisson's ratio [1], E is the Young's modulus (~231 x 10^3 MPa) [21], N = $d\ln\varepsilon/d\ln\sigma$ (which is 5 for Ni-35-12 and 6 for Ni-35-20 based on compression tests), $\sigma_y \cong 600$ MPa is the yield stress, σ_∞ is the flow stress at fracture, and $\varepsilon^P/\varepsilon_e$ is the ratio of plastic to elastic strain at fracture.

Using Chan's analysis [19], we estimate a fracture toughness for Ni-35-20 (inclusion size with ductile specimen of 100 μm) of ≈19 MPa$\sqrt{m}$ and a lower K_{IC}-value for Ni-35-12 (inclusion size ≈ 40 μm) of ≈15 MPa$\sqrt{m}$. All of these values are much higher than the 4-6 MPa$\sqrt{m}$ reported for NiAl at room temperature [22,23].

Figure 8 confirms the above estimates by showing results of chevron-notched short-rod fracture toughness tests for both Ni-35-20 and Ni-35-12. The results (from 3 tests of each alloy and all satisfying ASTM specifications for valid chevron-notch fracture toughness data) indicate K_{Iv} values of ~17MPa$\sqrt{m}$ for Ni-35-20, which is very close to that predicted above (19 MPa$\sqrt{m}$). The cast-and-extruded Ni-35-12 alloy exhibits an even higher fracture toughness of 22 MPa$\sqrt{m}$ or about 50% higher than predicted. Of primary interest is that all of the values are much greater than those (6 MPa$\sqrt{m}$) for NiAl using the same test procedure [23].

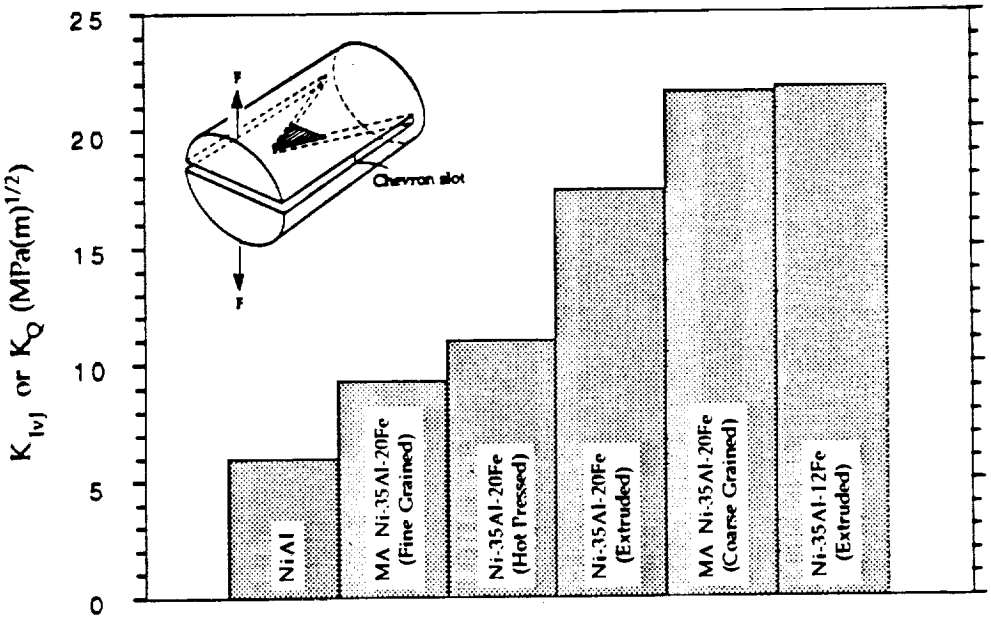

Figure 8. Room temperatrue fracture toughness values for cast and extruded NiAl-Fe alloys and NiAl-Fe+Y_2O_3 alloys processed by mechanical alloying. The grains sizes are as follows: NiAl (20μm), MA Ni-35-20 (Fine Grained) (2μm), Ni-35-20 (Hot Pressed) (28μm), Ni-35-20 (Extruded) (50μm), MA Ni-35-20 (Coarse Grain) (~800μm), and Ni-35-12 (Cast and Extruded) (45μm). Data for NiAl is from ref. 23.

It is interesting to note that the K_{IC} values in Figure 8 for the cast and extruded Ni-35-20 are much higher than the K_Q ≈ 11MPa$\sqrt{m}$ measured from notched bend bars of powder processed and hot-pressed material [15]. This is consistent with the low bend ductility (0.5%) of the hot-pressed Ni-35-20 previously mentioned in this text.

The enhanced toughness of the extruded NiAl + Fe alloys is consistent with the observation that room temperature ductility in NiAl alloys has only been observed in specimens in which hot extrusion is the final processing step. Several investigators have noted a strong <111> crystallographic texture produced in NiAl alloys during extrusion and have suggested that the texture is a major contributor to the observed ductility [24-26]. It is possible that aligning a tensile specimen parallel to <111> may decrease the uniaxial yield strength, and/or improve grain-to-grain compatibility at small strains, since three <100> {011} slip systems are highly stressed. However, crack growth in the present fracture toughness tests occurs parallel to the rod axis. Thus, the crack-tip stress field imposes the largest principal stress in a direction transverse to the <111>, not parallel to it as in a tensile test; furthermore, the stress state is multiaxial, not uniaxial. For this reason, we doubt that texture could benefit both tensile ductility and crack growth resistance on planes oriented at 90° to each other. We plan to report an analysis of this possibility in more detail at a later date.

D. Fracture of NiAl-Fe+Y_2O_3 Alloys Processed by Mechanical Alloying

The poor fracture resistance of polycrystalline NiAl at room temperature is well known. One possible route to improve the fracture toughness of NiAl-based alloys is to utilize mechanical alloying, MA. This was done in a previous study which indicated high toughness values in a MA Ni-35-20 + Y_2O_3 alloy [6]. However, those data, as well as other K_Q-values for NiAl [20], are based on through-thickness notched-bend specimens which were not precracked.

Given the difficulty of pre-cracking NiAl-based alloys and the relatively low toughnesses expected, short-rod, chevron-notched specimens have been used to obtain measurements of fracture toughness values [16]. In the present study, the tests were performed on material heat treated to single-phase B2 condition (see section A) and tested using the geometry shown in Figure 8. All of the data reported in Figure 8 for Ni-35-20 (extruded) and MA Ni-35-20 (coarse grained) are valid K_{IvJ} tests. The three MA Ni-35-20 (fine grained) tests all show similar values although only one satisfied ASTM specifications for K_{IvJ}; this result is reported. Based on these ASTM tests, Figure 8 also shows that the coarse-grained (~800μm) MA Ni-35-20 + Y_2O_3 alloy exhibits a fracture toughness value (K_{IC} = 21 MPa$\sqrt{m}$) comparable to the extruded Ni-35-12 alloy. In both cases the K_{IC} values are much higher than the values of 4 to 6 MPa$\sqrt{m}$ for NiAl. Furthermore, the high K_{IC} values are obtained in the MA materials despite their yield strengths of ~ 250 MPa higher than the Ni-35-20 alloy.

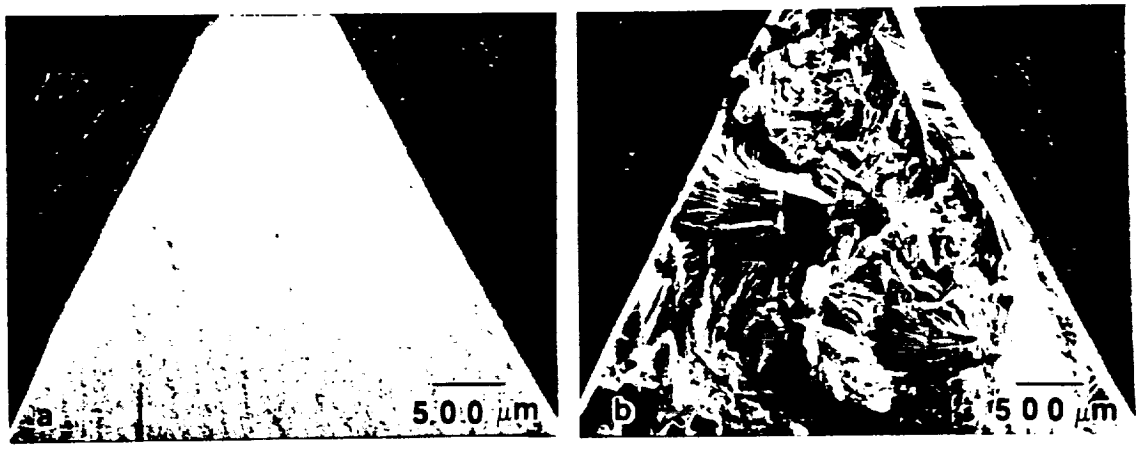

Figure 9. Fracture surfaces of Ni-35Al-20Fe+ Y_2O_3 processed by MA (a) before and (b) after the grain coarsening anneal. Samples tested by room temperature, Chevron-notched fracture toughness testing. Crack growth occurred from top to bottom in each micrograph.

In contrast to the comparatively "high" toughnesses above, the same MA Ni-35-20 alloy in the as-extruded, fine-grain condition (~2μm grain size) has a much lower K_{IC} value of only 9 MPa$\sqrt{m}$. The primary reason for the large grain-size induced differences in toughness is obvious in Figure 9 where the relatively flat fracture surface of the fine-grain material (Figure 9a) is supplanted by a very rough tortuous crack path (Figure 9b) in the coarse-grain MA Ni-35-20 + Y_2O_3. In the latter case, the fracture surface appears cleavage-like and crystallographic on a local scale with tear ridges prevalent (Fig. 9b). Thus, as in α-β Ti alloys where tortuous crack surfaces across a Widmanstätten microstructure result in improved toughnesses [27], the coarse-grained MA microstructure in this NiAl-based alloy also exhibits a much enhanced fracture toughness. Despite the presence of the oxide dispersoids, the large slip distances and relatively planar nature of slip within the single-phase beta matrix appear to contribute to the macroscopically tortuous crack path. It should be noted that the previous notched-bend tests [6], which reported a "high" toughness value of the fine-grained MA Ni-35-20 alloy apparently measured a large crack initiation energy in the notched, but not pre-cracked, specimens.

E. Elevated Temperature Flow Behavior

Slow strain-rate testing has been used to provide a preliminary assessment of the steady state creep response of the MA NiAl-Fe + Y_2O_3 alloys as a function of grain size. As shown in Figure 10, at 1000°C and a strain rate of $2x10^{-4}$ s^{-1}, the flow stress of both MA alloys is very sensitive to grain size, increasing rapidly with increasing grain size. After yielding, flow continues at more or less constant stress, which is consistent with steady-state behavior. It might be noted that under the same test conditions, Ni-50Al polycrystalline specimens with a grain size of 17 μm have a steady-state flow stress of ~45 MPa [26], or only slightly less than the MA Ni-35-20 + Y_2O_3 alloy with 5μm grain size at 1000°C. However, as has been discussed, the fracture toughness of the equiatomic NiAl alloy is only one-third of that of the coarse-grain (~800 μm) MA Ni 35-20 + Y_2O_3 alloy.

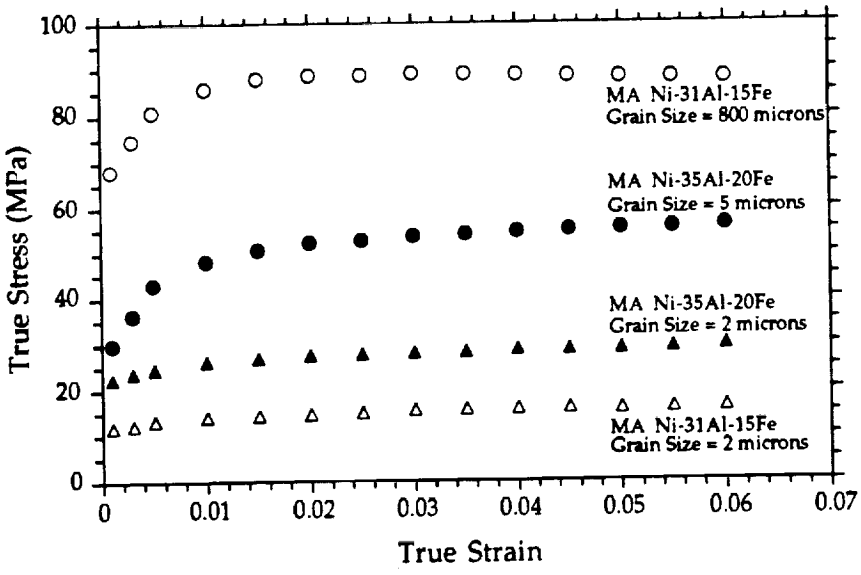

Figure 10. Compressive stress-stain response at 1000°C of mechanically alloyed NiAl-Fe+Y_2O_3 alloys as a function of grain size and matrix composition. Initial strain rate was $2x10^{-4}$ s^{-1}.

The steady-state flow stress behavior in Figure 10 permits an assessment of the secondary creep rate over a range of strain rates and stresses at 1000°C. As discussed elsewhere [14] and consistent with other MA alloys [29], we observe a strong influence of grain size not only on flow stress at a given strain rate but also on the creep stress exponent, $n = d\ln\dot{\varepsilon}/d\ln\sigma$. As expected, n increases with increasing grain size. However, most significant is the indication

that high n-values, typical of conventional, creep-resistant MA alloys [29], may be also achieved in this NiAl-based alloy. Specifically, the MA Ni-31-15 + Y_2O_3 alloy with ~800 μm grain size and elongated grain shape shows $n \simeq 12$ at 1000°C for the preliminary tests performed at compressive strain rates $2x10^{-5}\ s^{-1} \leq \dot{\varepsilon} \leq 2x10^{-3}\ s^{-1}$. This would be consistent with the existance of flow controlled by dislocation mobility which is hindered by interaction with Y_2O_3 particles. If such behavior can be retained to the low strain-rate regime ($<10^{-8}$/s), then relatively high creep strengths could be achieved. Such behavior will be examined in the future in the microstructurally stable Ni-35-12 alloy processed by MA with Y_2O_3 to provide oxide dispersion strengthening. Table II provides a summary of the grain sizes and creep stress exponents for the current alloys.

Table II. Grain Sizes and Creep Stress Exponents for the Current MA Alloys Tested in Compression at 1000°C ($2x10^{-5}\ s^{-1} \leq \dot{\varepsilon} \leq 2x10^{-2}\ s^{-1}$).

Material	Grain Size (μm)	$n = d\ln\dot{\varepsilon}/d\ln\sigma$
NiAl†	22	6
MA Ni-31-20	2	3
MA Ni-35-20	5	4
MA Ni-31-15	2	4
MA Ni-31-15	800*	12

†Data taken from Ref. 28.
*Maximum dimension in elongated grain structure (aspect ratio ~3).

Summary

The present results confirm the existence of room temperature ductility (~1 to 3% plastic strain) in single-phase B2 NiAl + Fe alloys in both ribbon and bulk (extruded) form. Furthermore, cast and extruded Ni-35Al-20Fe and Ni-35Al-12Fe can exhibit relatively high (17 to 22 MPa$\sqrt{m}$) fracture toughnesses. Our observations also indicate that certain compositions, such as Ni-35Al-20Fe, are susceptible to the formation of Fe-rich precipitates which not only age harden but also embrittle the alloy. Perhaps the most significant observation of this study is the presence of enhanced room temperature fracture toughness (≈21 MPa$\sqrt{m}$) as well as indications of improved elevated temperature creep resistance in grain-coarsened NiAl-Fe + Y_2O_3 alloys processed by mechanical alloying. While these results are preliminary, we note that there are very few, if any, existing approaches which offer a promise of improving both low temperature fracture resistance and elevated temperature creep resistance of NiAl alloys.

Acknowledgments

We wish to acknowledge several discussions and many useful suggestions by Dr. M. V. Nathal and Prof. L. Mulay. This research was supported by Inco Alloys International and by NASA Lewis Research Center.

References

1. D. B. Miracle, Acta Metall. Mater., 41 (1993) 649.

2. R. D. Noebe, R. R. Bowman and M. V. Nathal, Int. Metall. Rev. (in print).

3. R. Darolia, J. Met., 43 (1991) 44.

4. A. Inoue, T. Masumoto, and H. Tomioka, J. Mat. Sci., 19 (1984) 3097.

5. M. Rudy and G. Sauthoff, Mater. Sci. Eng., 81 (1986) 525.

6. J. Kostrubanic, D. A. Koss, I. E. Locci, and M. Nathal, in High Temperature Ordered Intermetallic Alloys IV, MRS Symp. Proc. Vol. 213, (MRS, Pittsburgh, 1991) p. 673.

7. S. V. Raj, I. E. Locci and R. D. Noebe, Metall. Trans., A 23A (1992) 1705.

8. S. Guha, P. Munroe, and I. Baker in High Temperature Ordered Intermetallic Alloys III, MRS Symp. Proc., Vol. 133, (MRS, Pittsburgh, 1991), p. 633.

9. M. Larsen, A. Misra, S. Hartfield-Wünsch, R. Noebe, and R. Gibala in Intermetallic Matrix Composites, MRS Symp. Proc., Vol. 194, (MRS, Pittsburgh, 1990), p. 191.

10. K. Vedula, G. M. Michal, and A. M. Figueredo, Modern Developments in Powder Metallurgy, 20 (1988) 491.

11. M. Dollar, S. Dymek, S. J. Hwang, and P. Nash, Scripta Met., 26 (1992) 290.

12. S. Dymek, M. Dollar, S. J. Hwang, and P. Nash, Mater. Sci. and Eng. A, 152 (1992) 160.

13. S. Dymek, M. Dollar, S. J. Hwang, and P. Nash in High Temperature Ordered Intermetallic Alloys V, MRS, Pittsburgh (in print).

14. J. Breedis, D. A. Koss, J. Poole, and I. Locci, to be published in Proc. 2nd Int. Conf. on Structural Applications of Mechanical Alloying (ASM, Metals Park, 1993).

15. J. Kostrubanic, M.S. Thesis, The Pennsylvania State University, 1991.

16. ASTM E 1304-89, Annual Book of ASTM Standards, Vol. 03.01, (ASTM, Philadelphia, 1990), p. 940.

17. A. J. Bradley, J. Iron Steel Inst., 168 (1951) 233.

18. S. Guha, P. Munroe, and I. Baker, Scripta Metall., 23 (1989) 897.

19. K. S. Chan, Scripta Metall. Mater., 24 (1990) 1725.

20. N. E. Dowling, Eng. Frac. Mech. 26 (1987) 333.

21. M. R. Harmouche and A. Wolfendun, J. Test. Eval., 15 (1987) 101.

22. S. Reuss and H. Vehoff, Scripta Metall Mater., 24 (1990) 1021.

23. K. S. Kumar, S. K. Mannan, and V. Viswanadham, Acta Metall Mater., 40 (1992) 1201.

24. K. H. Hahn and K. Vedula, Scripta Metall., 23 (1989) 7.

25. E. P. George and C. T. Liu, J. Mater. Res., 5 (1990) 754.

26. P. S. Khadkikar, G. M. Michal, and K. Vedula, Metall. Trans. A, 21A (1990) 279.

27. H. Margolin, J. C. Williams, J. C. Chesnutt, and G. Lutjering in Titanium '80, Vol. 1 (TMS, Warrendale, 1980) p. 169.

28. J. D. Whittenberger, J. Mater. Sci., 22 (1987) 394.

29. E. Arzt, Res. Mechanica, (1991) 399.